NATIONAL ADVISORY COMMITTEE FOR AERONAUTICS

TECHNICAL NOTE 3668

PRELIMINARY INVESTIGATION OF A FAMILY OF DIFFUSERS DESIGNED FOR NEAR SONIC INLET VELOCITIES

By Richard Scherrer and Warren E. Anderson

Ames Aeronautical Laboratory
Moffett Field, Calif.

Washington
February 1956

NATIONAL ADVISORY COMMITTEE FOR AERONAUTICS

TECHNICAL NOTE 3668

PRELIMINARY INVESTIGATION OF A FAMILY OF DIFFUSERS DESIGNED FOR NEAR SONIC INLET VELOCITIES

By Richard Scherrer and Warren E. Anderson

SUMMARY

Tests have been conducted with a series of diffuser shapes defined by empirical equations having constants which are related to the initial boundary-layer thickness. The shapes were designed to provide high pressure recovery at near sonic inlet Mach numbers, and tests were conducted through the mass-flow range with a variety of attached and separated initial boundary layers. Tests were also conducted with two offset ducts and with a variety of surface conditions in the shortest duct.

The experimental results provide substantiation for the design trends upon which the empirical equations were based. In addition, it was found that for the axially symmetric ducts tested, the effect of initial boundary-layer thickness on pressure recovery was as important as that of duct shape. The best performance was obtained with a short duct with a thin initial boundary layer. With separated boundary layers, extended entry lengths provided markedly improved pressure recovery and flow steadiness relative to a similar duct with no entry extension. The offset ducts suffered losses in all performance parameters relative to a similar axially symmetric duct. Near maximum mass flow, the surface conditions investigated had only small adverse effects on pressure recovery. A loss of several percent in total pressure recovery occurred with air leakage into the duct near the throat.

INTRODUCTION

Although numerous investigations of the performance of subsonic diffusers have been made over a period of years, the need for efficient air-induction systems for the turbojet and ram-jet engines of supersonic aircraft has caused a demand for further research on this classic problem.[1] With efficient methods of supersonic compression, the initial Mach number

[1]A review of the history of diffuser research is given in reference 1.

in a subsonic diffuser is high (≥ 0.8) and positive pressure gradients can be large. Also, there exists an initial boundary layer at the duct entrance which can be thin, thick, or separated. To achieve the high levels of flow uniformity, steadiness, and pressure recovery required by jet engines, considerable care must be exercised in the layout of ducts to insure that high positive pressure gradients which cause separation are avoided and, in the case of initially separated flow, that reattachment will occur in the subsonic diffuser.

Almost all experiments with isolated subsonic diffusers have been conducted with units having constant divergence angles and usually only pressure recovery has been measured. Notable exceptions are the investigations of references 2, 3, and 4 in which extensive static-pressure distributions and numerous boundary-layer profiles were measured in large conical diffusers. In the design of subsonic diffusers for supersonic air-induction systems, it is also necessary to have knowledge of the geometric and flow variables affecting flow uniformity and flow steadiness in addition to knowledge of factors affecting pressure recovery.

Numerous studies have been made using turbulent boundary-layer theory to obtain efficient diffuser shapes for incompressible two-dimensional and axially symmetric flows. However, as shown in reference 5, existing turbulent boundary-layer theory in compressible flow is not sufficiently refined for design purposes because the effects of positive pressure gradients are not known with sufficient accuracy. As a result, a variety of methods has been applied in the design of actual duct installations. For the most part, these duct shapes are simply fairings, based on experience, from the inlet to the exit after these areas have been located and their sizes calculated. Because of the almost infinite number of possible fairings, combined with the number of possible combinations of initial conditions, it is difficult to design an efficient duct shape for given operating conditions from existing data. When the additional considerations of off-design operation, and weight and volume limitations are included in the duct problem, it becomes doubly difficult to obtain an efficient duct. The purposes of the present preliminary investigation were: (1) to provide information for more systematic diffuser design by developing an empirical general equation for the radius distribution of axially symmetric diffusers, (2) to select coefficients for the general equation from study of available theory and experiment, and (3) to make measurements of pressure recovery, flow uniformity, and flow steadiness in several of the resulting diffusers. The experiments are exploratory in nature and serve to indicate qualitative agreement between the design trends upon which the empirical equations are based and the performance of the empirical duct shapes. The investigation also included measurement of some effects of duct center-line offset and surface conditions to determine the order of magnitude of these effects.

NOTATION

A	cross-sectional area
a	exit slope ($\tan \theta^{\circ}_4$) (See sketch p. 4.)
b	function of $\frac{\theta_{2'}}{r_{2'}}$
c	entry length in terms of inlet radii
e	Napierian constant
H	boundary-layer profile shape parameter, $\frac{\delta^*}{\theta}$
K	arbitrary constant
M	Mach number
m	mass flow, $\rho \bar{V} A$
$m_{2'}*$	maximum mass flow based on choked, isentropic entrance conditions
p	static pressure
q	dynamic pressure
p_t	total pressure
Δp	static-pressure fluctuation
Re	Reynolds number
r	radius
S	constant in equation (2)
u	local velocity within boundary layer
U	local velocity immediately outside boundary layer
$\bar{V}$	average velocity
V_m	maximum velocity at station 3
X	$K \frac{x}{r_{2'}}$

x	distance downstream from minimum area station
Y	distance from reference surface or center line
δ	boundary-layer thickness
δ^*	boundary-layer displacement thickness
θ	boundary-layer momentum thickness
θ°	half of diffuser divergence angle
ρ	mass density

Subscripts

∞	ambient conditions
l	local conditions
1	bellmouth entrance station
2'	subsonic diffuser entrance (minimum area) station
3	rake measuring station (compressor inlet)
4	exit station

DIFFUSER-SHAPE EQUATIONS

A study of available theory and experiment has indicated that at least four geometric variables must be included in an equation to define a family of reasonable diffuser shapes which are to have near sonic entrance Mach numbers. These variables are illustrated in the following sketch:

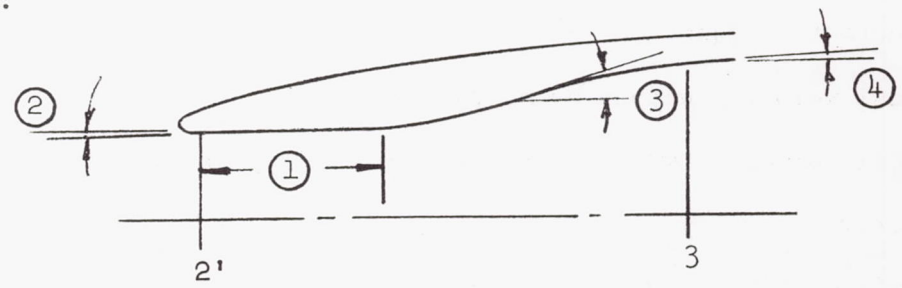

(1) Entry length
(2) Initial slope
(3) Maximum slope
(4) Exit slope

The entry length is a region of nearly constant cross-sectional area and, as will be discussed in detail later, has been found to be essential in some duct systems. From a study of test data for diffusers with various initial flow conditions, duct shapes were generally found to require a change in wall slope from the initial to the maximum and final values when flow separation is to be prevented. A criterion for avoiding separation in two-dimensional incompressible flow is that separation will never occur when the boundary-layer shape parameter H ($H = \delta^*/\theta$) is equal to or less than 1.8 (see ref. 6). This condition has been assumed and is fundamental in the empirical evolution of the shape equations and evaluation of the constants which are discussed in detail later in this report.

It is possible to describe diffuser shapes, such as that shown in the sketch, with many different equations, but an exponential polynomial form was found to be most convenient. It was also found convenient, and reasonable in the light of existing data, to use two equations to describe diffuser shapes. The first equation defines the longitudinal distribution of local radius of an axially symmetric diffuser as dictated by the desired initial, maximum, and final slopes. The second equation is arranged to provide desired entry lengths by an exponential stretching of the ordinate spacings in the upstream direction. These equations are:

$$\frac{r}{r_{2'}} = 1 + \frac{a}{K}\left(X + \frac{1}{2}e^{-2X} - \frac{1}{2}\right) + \frac{b}{2K}\left(1 - e^{-X^2}\right) \tag{1}$$

where

X $K\dfrac{x}{r_{2'}}$

a exit slope

b function of $\theta_{2'}/r_{2'}$

K constant

and

$$\left(\frac{x}{r_{2'}}\right)_{\text{extension}} = \left(\frac{x}{r_{2'}}\right)_{\text{eq.(1)}} - ce^{-S\left(\frac{x}{r_{2'}}\right)_{\text{eq.(1)}}} \tag{2}$$

where

c entry length extension in terms of inlet radii

S constant

In these equations, the exponents were selected by inspection of diffuser contours resulting from calculations utilizing various combinations of exponents. The constants S, K, a, and b have been evaluated by a study of available data in conjunction with the empirical equation to provide satisfactory diffuser shapes. The initial slope of the curves defined by equation (1) is zero; the reasons justifying the selection of this value will be discussed subsequently.

The need for some entry length is indicated by the results of references 7 through 10. Extended entry regions as great as 3 inlet diameters in length have been shown to provide steady flow for wide ranges of mass-flow ratio at both subsonic and supersonic speeds. The reason for extending the entry of a diffuser is to provide a region of nearly uniform pressure in which the boundary-layer shape parameter H can reduce to a value for which the subsequent diffuser was designed. Equation (2) provides for the forward extension of a diffuser shape, from equation (1), by any desired amount through selection of a value of the constant c. Since there is only a qualitative link between the initial boundary-layer conditions and the value of c, it is necessary to determine the best value for a given duct system by judgment and experiment. The value of S in the exponent of e in equation (2) was selected so that the maximum and exit slopes would remain essentially unchanged when the entry length was extended (S = 5). A lower value of S would result in a reduction in maximum slope with increasing entry length.

The selection of a zero value of initial slope is justified qualitatively by reference to one-dimensional flow relations. It can be shown that when the flow at the entry is near sonic the rate of area change with length must be near zero to prevent large positive pressure gradients. Also, experimental pressure distributions shown in reference 11 indicate that to prevent the formation of a local supersonic region near the wall at the entry to even a low-angle conical diffuser, it is necessary to use a low initial divergence angle ($\theta^\circ \approx 1^\circ$). Another investigation of the flow at the entry to a 10° included-angle conical diffuser (ref. 3) shows that to prevent the formation of a supersonic region at the throat, a circular-arc fairing with a radius of at least eight times the throat radius was required. Seddon (ref. 12) also discusses the advantages of a low value of initial slope and some entry length to provide the best pressure recovery in subsonic nose inlets for wide ranges of inlet velocity ratio. The requirements of a near zero initial slope and a gradual fairing to the maximum slope are satisfied by equation (1) and are unaffected by equation (2).

A region of maximum slope exists because as the flow is decelerated from near sonic speed, the wall slope increases for a constant positive pressure gradient. The practical maximum slope is limited by boundary-layer separation and must be related to the initial boundary-layer thickness. Such a relation is obtained from the theory of reference 13 and, for a constant value of H, the relationship is

$$\tan \theta^{\circ}_{max} = \text{constant}\left[\frac{r_{2'}}{\theta_{2'}(Re_{\theta_{2'}})^{1/6}}\right] \tag{3}$$

Since the variation in $(Re_{\theta_{2'}})^{1/6}$ is small between usual models and full-scale aircraft flying at high altitudes (the condition of maximum $\theta_{2'}$), the parameter $r_{2'}/\theta_{2'}$ is probably sufficient for correlation of test results. It has been used frequently in the past. Examination of experimental data (ref. 2) and calculations using relations from reference 13 indicate that a reasonable relationship between the initial boundary-layer conditions and the maximum divergence angles is

$$\frac{1}{\theta^{\circ}_{max}} = 0.133 + 9.1\frac{\theta_{2'}}{r_{2'}} \tag{4}$$

The form of this equation is obtained from the theory of reference 13. The constants were evaluated by plotting in the form $\frac{1}{\theta^{\circ}_{max}}$ vs. $\frac{\theta_{2'}}{r_{2'}}$ the data from reference 2 (where θ° was measured using $(r - \delta^*)$ as wall ordinates) and from calculations for $H = 1.8$ based on reference 13. In applying equation (1), it is necessary to express the parameter b in terms of $\theta_{2'}/r_{2'}$ and this expression, based on equation (4) as a boundary condition, is a complex expression which can be approximated by the relation

$$b = 0.1942 - 6.42\frac{\theta_{2'}}{r_{2'}} \tag{5}$$

The difference between the maximum slope as given by equation (4) and as finally obtained by equations (1) and (5) is less than $\pm 0.5^{\circ}$. Duct models for two values of $\theta_{2'}/r_{2'}$ were used in the present investigation. These and the corresponding values of maximum divergence half angle and b are tabulated below

$\theta_{2'}/r_{2'}$	θ_{max}, deg	b
0.0045	5.75	0.165
.022	3	.053

These values were selected as representative of diffusers with thin and thick boundary layers.

The exit slope, the constant a in equation (1), is indicated by both theory and experiment to be less than the maximum slope for diffusers with area ratios of the order of 2:1. The theoretical diffuser contours developed in references 7 and 13 required a gradual reduction in slope

with increasing length to maintain a constant H. In tests of conical diffusers (refs. 2, 3, and 4) with high subsonic values of $M_{2'}$, H was found to increase rapidly toward the exit. These results indicate that if H is to be constant, the pressure gradient must be reduced more rapidly toward the exit than is possible with a conical duct; thus, the exit slope should be less than the maximum slope. Available data for values of $(r - \delta^*)$ as a function of x for the conical diffusers of references 2 and 4 indicate that a reasonable exit slope is from 2° to 3°. This range is so narrow that the exit slope is considered to be constant and the value of a was selected as 0.035, which is the tangent of 2°.

The exit slope, as well as the maximum slope expressed by equation (4), does not include corrections to offset the effects of boundary-layer growth. Experimental measurements of δ^* in conical diffusers (refs. 2 and 4) indicate that the effect of boundary-layer growth can be taken into account approximately by a constant incremental wall-divergence angle of from $1/2^\circ$ to 1° except near the exit. Near the exit, the growth of δ^* was unusually rapid and as a result, H became very large. However, in the present investigation of diffusers with a reduction in wall slope toward the exit, and with a maximum slope of 10° or 12°, use of a constant divergence half-angle of 1° for boundary-layer compensation was considered satisfactory. As a result, the total divergence angles for the two values of $\theta_{2'}/r_{2'}$ become 13.5° and 8°. This incremental angle was added to the wall contours after the contours had been calculated by equations (1) and (2); thus, all duct models had an initial total divergence angle of 2°. The constant K in equation (1) determines the value of $x/r_{2'}$ at which the wall contour closely approximates the selected exit slope. This condition, as indicated by inspection of a family of curves, occurs at $K(x/r_{2'}) = 2.0$. For the diffuser models it was decided that the wall slope should reduce to the exit slope when the duct cross-sectional area is twice the entrance area. These boundary conditions result in the value of K being 0.326 for the 13.5° diffusers.

APPARATUS AND TEST

Ducts

One of the ducts of this series of tests is shown mounted on an air intake pipe in the photograph of figure 1, and the general arrangement of the test apparatus is shown in figure 2. Seven ducts were constructed of Fiberglas and polyester resin and an eighth model was machined from an aluminum casting.

The duct contours are designated by a numbering system that consists of the maximum total divergence angle (including boundary-layer compensation) and the throat extension in inlet radii. Five of the seven ducts had the following axially symmetric shapes:

1. 13.5° - 0
2. 13.5° - 2
3. 13.5° - 6
4. 8° - 2
5. 8°c - 0.5

The 8°c - 0.5 was a conical duct with an entrance extension providing an initial contour about the same as the 13.5° - 0 duct. This conical duct was included in the test program for comparison purposes and because the shapes defined by equation (1) approach the conical for thick boundary layers. The 8°c - 0.5 duct contour is nearly identical to an 8° - 0 shape except that the exit divergence of the 8° - 0 duct would be 6° rather than 8°. The ordinates of the five axially symmetric ducts are shown in figure 3 and those of two offset ducts, having the 13.5° - 2 basic shape, are shown in figure 4. The center-line shapes of the offset ducts were similar to the wall contour of the 13.5° - 2 duct. All ducts tested had throat-station radii equal to 1.50 inches.

The cast aluminum duct was made with the 13.5° - 0 shape and was used to illustrate effects of surface roughness and waviness. Effects of air leakage into the duct were determined with the 13.5° - 0 Fiberglas duct. The initial surface of the aluminum duct was machined, polished, painted, and repolished to as smooth a finish as could be obtained. The revisions to this surface finish and the details of the leakage-hole locations in the Fiberglas model are discussed later with the presentation of the test data.

Instrumentation

Measurements were made of total-pressure recovery, mass-flow ratio, exit-flow uniformity, axial static-pressure distribution, entrance Mach number, entrance boundary-layer thickness, and the degree of flow unsteadiness. The locations of total- and static-pressure tubes in the ducts are shown in figure 2. The average total-pressure ratio was obtained by the mass-derived method as discussed in reference 14. The values of diffuser static pressure necessary in using this method were obtained by averaging rake and wall static-pressure measurements. The exit total-pressure rake was located at the values of $x/r_{2'}$ for which the area ratio, $A_{2'}/A_3$, was 0.51 for all the ducts tested (see fig. 3). Alternate and possibly more desirable locations would be at values of $x/r_{2'}$ for equal flow velocities on the duct center line at a given mass flow in all models. These values of $x/r_{2'}$, in theory are those for a fixed area ratio in the duct contours without boundary-layer compensation. However,

location of the exit rake at these stations requires more confidence in the method of boundary-layer compensation than appears justified, and, as a result, the rake was located as indicated in figure 2. The quantity of air flow was measured by a standard A.S.M.E. orifice meter downstream of the test duct. In addition, a small adjustable total-pressure probe in conjunction with a surface static tube was used to measure the boundary-layer velocity profiles at one point near station 2'. The probe and a micrometer height gage which was adapted for surveying thin boundary layers allowed measurements to within 0.012 inch of the surface. A piezoelectric pressure cell together with an oscillograph was used to measure the amplitude of static-pressure oscillations in the flow at the duct exit. The pressure-cell instrumentation had essentially linear response in the frequency range from 0 to 3000 cycles per second.

The exit-velocity distributions measured in the present investigation were compared with those presented in reference 14 in which an analysis was made of the accuracy of various methods of calculating total-pressure recovery and the extent to which the accuracy may be affected by exit-velocity distribution. The comparison indicated that at a mass-flow ratio of 0.95, the maximum difference between the total-pressure recoveries presented herein and those which could be calculated by the most exact method of reference 14 should be only about 0.25 percent. The values of static-pressure unsteadiness corresponding to the measured exit-velocity distributions in the straight ducts were found to be consistently less than about 1-1/2 percent of ambient total pressure. It is assumed that when the value of flow unsteadiness is less than this amount the inaccuracies of total-pressure measurements are equal to those in steady flow. A gradual deterioration of accuracy is to be expected with increasing flow unsteadiness.

Tests

Preliminary tests were conducted to develop a technique for obtaining desired boundary-layer thicknesses at the diffuser entrance (minimum area station). It was found that a series of wire rings about 1 inch apart upstream of the throat would produce adequately thickened boundary layers up to $\theta_{2'}/r_{2'}$ of about 0.016. Greater values resulted in a deterioration in repeatability and were not used. As a result, the 8° ducts were not tested at the design value of $\theta_{2'}/r_{2'}$ which was 0.022. Wires of several different diameters from 0.032 to 0.125 inch were used and considerable care in wire installation was required to obtain adequately repeatable boundary-layer surveys. The boundary-layer thickness decreased only slightly with increasing throat Mach number. The table below lists the trip-wire sizes and their locations for the profiles used in the present investigation (shown in fig. 5).

Attached flow			
	$\theta_{2'}/r_{2'}$	Wire location, in. upstream from station 2'	Wire diameter, in.
A	0.00143		No wire
B	.00826	1.25	0.040
C	.01560	0.75, 1.25, 2.25	0.040
Separated flow			
	$\delta^*/r_{2'}$	Wire location, in. upstream from station 2'	Wire diameter, in.
D	0.0147	0.25	0.030
E	.0600	At station 2'	.062
F	.0906	At station 2'	.125

In order to obtain separated boundary layers, it was necessary to locate the wire ring at or just ahead of the minimum-area station 2'. With such a wire location, reattachment was apparently controlled by the magnitude of the initial divergence in the diffuser. In the case of the thinnest separated boundary layer (designated D in fig. 5) reattachment had already occurred ahead of the probe measuring station. The momentum thicknesses of the attached profiles and the displacement thicknesses of the separated profiles are tabulated in figure 5. The displacement thickness of the separated profile has been used in preference to the momentum thickness because displacement thickness increases consistently with increased depth of the separated region. The reverse flow velocities in the separated portion of the boundary layers were not measured, and, as a result, the reverse velocities were assumed to be zero in computing displacement thickness.

RESULTS AND DISCUSSION

The range of inlet Mach numbers of primary interest in the present investigation is between 0.77 and 1.0. A Mach number of unity would occur in an optimum supersonic inlet with isentropic flow while a Mach number of 0.77 is that which exists behind a normal shock wave at a free-stream Mach number of 1.3. The static-pressure-rise ratio for this normal shock wave is approximately that which will separate a turbulent boundary layer (see ref. 15) and thus 0.77 represents a lower limit of $M_{2'}$ without separation of the initial boundary layer.

Three curves have been prepared to facilitate interpretation of the test data. In figure 6, mass-flow ratio is plotted as a function of inlet Mach number $M_{2'}$ for the three attached boundary-layer inlet conditions. The $M_{2'}$ range of primary interest as discussed above is also denoted in the figure. The plot of a flow-uniformity parameter $V_m/\bar{V}_3$ as a function of total-pressure ratio p_{t_3}/p_{t_∞} is shown in figure 7. The curves of figure 7 were obtained by employing the assumptions that the total-pressure recovery at some point near the duct center at station 3 was equal to p_{t_∞} and that the static-pressure variation across station 3 was negligible (see Appendix). These conditions are satisfied at mass-flow ratios up to that at which the flow unsteadiness exceeds 1-1/2 to 2 percent of p_{t_∞} for all except the offset ducts. Inlet total-pressure ratios are presented in figure 8 for the various entry conditions. These values, when combined with the pressure ratios in figures 9, 17, and 18 for corresponding mass-flow ratios, provide the values of p_{t_3}/p_{t_∞} necessary to obtain indications of flow uniformity from figure 7. The curves of figure 7 show that only small losses in total pressure are acceptable if a low value of the uniformity parameter $V_m/\bar{V}_3$ is to be maintained.[2] It should be noted that the curves of figure 7 were obtained by the use of mass-derived values of p_{t_3}.

For simplicity of presentation the discussion is divided into the following four subheadings:

1. Axially symmetric ducts with attached initial boundary layers
2. Axially symmetric ducts with separated initial boundary layers
3. Ducts with offset axes
4. Surface conditions

Axially Symmetric Ducts With Attached Initial Boundary Layers

The total-pressure ratios obtained in tests of the five axially symmetric ducts for three values of $\theta_{2'}/r_{2'}$ are presented in figure 9. Corresponding values of the more conventional total-pressure loss

[2]The duct area ratio ($A_{2'}/A_3 = 0.510$) results in the maximum Mach number at the diffuser exit, $M_3 \sim 0.3$, being less than that for a typical turbojet engine, $M_3 = 0.4$ to 0.5, in which $V_m/\bar{V}_3$ should be less than 1.2. The allowable pressure loss for $V_m/\bar{V}_3 \leq 1.2$ would be greater for ducts with higher maximum values of M_3. The allowable values of $V_m/\bar{V}_3$ for ram-jet engines, which use lower values of M_3, have not been established.

coefficient $(p_{t_3} - p_{t_{2'}})/q_{2'}$ are given in figure 10 for comparison with results of other diffuser investigations. In making such comparisons one should recognize the effects of the averaging methods on the values of total-pressure ratio. (See ref. 14.)

The effect of initial boundary-layer momentum thickness on total-pressure ratio is most clearly illustrated by a cross plot of figure 9. Such a cross plot for $M_3 = 0.3$ is shown in figure 11. The total-pressure ratios are apparently as sensitive to initial boundary-layer conditions as to the range of duct shapes that were investigated. For thin initial boundary layers the change of pressure recovery due to duct shape was greater than for thick boundary layers. The use of extended entry sections resulted in lower values of pressure ratio for thin boundary layers as can be seen by the trend of the curves for the 13.5° - 0, 13.5° - 2, and 13.5° - 6 ducts. These results and the empirical equations indicate that for a thin initial profile the flow should be diffused rapidly. This, of course, suggests removing the boundary layer at the diffuser entry. It is possible that reducing maximum slope with increasing entry length, by using a lower value of S in equation (2), could provide improved pressure recovery. Although tests were not conducted at the greater design value of $\theta_{2'}/r_{2'}$, 0.022, the results shown in figure 11 indicate that the 8° - 2 duct could be better than the others with thick boundary layers even though some entry extension was used.

The longitudinal static-pressure distributions of the ducts for $M_3 = 0.3$ are shown in figure 12. It is of importance that the initial rapid rise in pressure that is most apparent with the longest duct (13.5° - 6) was found, by assuming one-dimensional flow, to be due to the 1° incremental divergence angle for boundary-layer compensation. Thus, the need for zero initial slope to maintain low initial pressure gradients is evident. In view of the effect of the method of boundary-layer compensation on the pressure gradient, it is apparent that the boundary condition of $(dr/dx)_{2'} = 0$ should be imposed in compensation methods as well as in duct contour equations.

The flow steadiness results shown in figure 13 indicate that the flow is never steady at the higher mass-flow ratios ($m_{2'}/m_{2'}^* > 0.50$). The maximum total amplitude, and also the frequency,[3] increase steadily with increasing mass-flow ratio. The uniformity of the total-pressure profiles in figure 14 indicates that the basic oscillation is probably not due to flow separation which also indicates that the exit slope was not too large. Increasing boundary-layer thickness resulted in greater unsteadiness and, occasionally, single high-amplitude oscillations would occur. In some models a definite beat frequency of rising and falling

---

[3]The predominant frequency increased to a maximum value of approximately 1200 cycles per second at $m_{2'}/m_{2'}^* \rightarrow 1.0$.

amplitude was indicated and was audible as well. The maximum amplitudes of these oscillations are indicated as solid symbols in figure 13.

The flow uniformity parameter $V_m/\bar{V}_3$ was calculated for the flow shown in figure 14(a) to indicate the level of uniformity attained at high mass-flow ratios with the thinnest boundary layer. Both direct integration of the local velocities and use of figures 7 and 8 result in $(V_m/\bar{V}_3) = 1.21$ at the mass-flow ratio of 0.980. At lower mass-flow ratios the flow is more uniform. All the other ducts, however, had higher values of $V_m/\bar{V}_3$ at equivalent percentages of the maximum mass-flow ratio with the thinnest boundary layer and had still higher values with thicker boundary layers.

The best duct shape of those investigated with a thin attached initial boundary layer is apparently the 13.5° - 0 shape. However, an increase in initial boundary-layer thickness causes a rapid reduction in total-pressure ratio and the 8°c - 0.5 duct becomes the best. With thick boundary layers the 8° - 2 duct appears best. This trend is in agreement with the trends upon which equation (1) and the constants were based. A significant conclusion of this portion of the investigation is that the initial boundary-layer thickness is as important as the wall contour in determining the pressure recovery, flow uniformity, and flow steadiness at high mass-flow ratios.

Axially Symmetric Ducts With Separated Initial Boundary Layers

Ducts with a maximum divergence angle of 13.5° were tested with three thicknesses of separated initial boundary layers. The total-pressure ratios attained in these tests are shown in figure 15 and a cross plot at a constant value of diffuser discharge Mach number of 0.25 is shown in figure 16. The high pressure recoveries for the 13.5° - 6 duct at $(\delta^*_{2'}/r_{2'}) = 0.06$ are consistent with the low values of the static-pressure fluctuations shown in figure 17. It is apparently possible, with long entry lengths, to attain as low values of flow unsteadiness with initial separation as are attained with unseparated flow. The general shape of the curves in figure 16 and comparison with the total-pressure ratios for thin attached initial boundary layers indicates that entry length has a favorable effect when the initial boundary layer is separated. The rapid reduction in total-pressure ratio at large values of $\delta^*_{2'}/r_{2'}$, however, suggests that there is a practical limit to the value of δ^*/r that can be allowed in inlet design.

Ducts With Offset Axes

The total-pressure ratios attained with the offset ducts are shown in figure 18, and it is apparent that the offsets have caused substantial additional losses relative to the axially symmetric duct. As shown by a comparison of figures 19 and 13, the pressure loss for the duct with the r_2' offset is accompanied by at least doubled values of flow unsteadiness ($\Delta p_3/p_{t_\infty}$) at most mass-flow ratios. Exit velocity distributions indicate that some separation always occurred in the offset ducts. As a result, the flow uniformity at high mass-flow ratios in both offset ducts had values greater than $V_m/\bar{V}_3 = 1.5$.

Tests were also conducted with semicircular boundary-layer-thickening wires located so as to affect only the steeper side of the duct (upper surface in fig. 4). The amplitude of flow oscillations with these circumferentially nonuniform boundary-layer thickness distributions were essentially identical to those obtained with equal size annular wires as shown in figure 19. The performance of the offset ducts is obviously affected by the choice of shape and mean-line contour, and it is probable that somewhat better shapes than those tested are attainable for the same length and offset.

Surface Conditions

The investigation of surface conditions was conducted with the 13.5° - 0 duct shape, and several roughnesses, waviness amplitudes, and leakage conditions were investigated. The results obtained with the thinnest attached boundary layers are shown in figures 20 and 21. Results obtained with thicker boundary layers with each surface condition showed some reduction in the adverse effects. Since the measured effects of surface conditions were small, only the data for the thinnest boundary layer are presented.

Surface roughness.- The range of roughness investigated was from the smooth polished aluminum model to a surface with discrete circumferential ridges throughout the duct (fig. 20(a)). These ridges were produced by tape strips. The tape was 0.003 inch thick and 3/4 inch wide and was placed in circumferential strips at numerous positions in the duct. The tape thickness was 1.4 times the momentum thickness of the boundary layer at the throat. The dimensions of the sanded roughness and slight waviness in the models indicated in figure 20(a) were not measured. The sanded roughness was definitely perceptible to the touch. The slight waviness was due to nonuniform shrinkage of the polyester resin from which the model was made and was very perceptible when viewed with a light shining axially through the duct. The effects of this range of surface conditions amounted to about 1 percent reduction in pressure recovery.

Surface waviness.- The effect of duct-wall deflections throughout full-scale ducts under internal pressure loads was simulated as shown in figure 20(b). It was assumed that the duct shell would deflect between rigid circumferential stiffeners, and wave amplitudes (model scale) of 0, 0.010, 0.020, and 0.040 inch were used. Increasing waviness caused the small reduction in pressure ratio shown in figure 20(b); however, some change in flow unsteadiness is shown in figure 21. The flow uniformity was little affected.

Air leakage into duct.- The leakage investigated occurred through groups of 1/32-inch-diameter holes drilled at about 3/32-inch spacings at each duct station as shown in figure 20(c). Leakage into the downstream part of the duct had little effect on pressure recovery. A significant reduction in total-pressure ratio occurred at high mass-flow ratios when leakage was allowed near the throat as well as in the downstream region.

Summary of surface-condition tests.- It was anticipated that the 13.5° - 0 duct would be particularly sensitive to surface conditions because of the large maximum divergence angle. However, the results, particularly with roughness and waviness, resulted in unexpectedly small variations in pressure recovery. It appears likely that this result is related to the measured increase in flow uniformity with increasing extent of surface roughness reported in reference 16.

CONCLUDING REMARKS

The experimental results of the present investigation provide substantiation for the design trends, upon which the empirical equations were based, as follows:

1. When the entry flow was nonuniform, that is, separated boundary layer, extended entry lengths resulted in better pressure recovery, as well as more steady and uniform flow at the duct exit station.

2. The initial slope must be zero for near sonic entry conditions for the duct contour with or without boundary-layer compensation to have low initial pressure gradients.

3. The empirical interrelationship of the parameter $\theta_{2'}/r_{2'}$ and the maximum divergence angle, that was used in deriving the duct shapes, provided high pressure recovery and steady uniform flow at high mass-flow ratios when the initial boundary layers were thin. With the thickest boundary layer the diffuser shapes provided by the empirical relations are near conical and provide at least as good performance as low-angle conical diffusers.

4. Although the exit slope was not a variable in the present investigation, the fact that steady uniform flow was obtained in the 13.5° - 0 duct at high mass flows with thin initial boundary layers indicates that the exit slope was not too large.

Other results of the experimental investigation are:

1. For the axially symmetric models, the effect on total-pressure ratio of initial boundary-layer thickness was found to be as great as that of the range of duct shapes investigated. This, of course, indicates the advisability of maintaining thin initial boundary layers to allow use of short diffusers.

2. The offset ducts of the present investigation suffered losses in all performance parameters relative to the equivalent axially symmetric diffuser. As a result, it appears advisable to minimize the offset in duct design.

3. The effects of the surface conditions investigated on the losses in total-pressure ratio were not large. The largest losses occurred with air leakage into the duct near the entry.

Ames Aeronautical Laboratory
National Advisory Committee for Aeronautics
Moffett Field, Calif., Sept. 6, 1955

APPENDIX

FLOW UNIFORMITY

In subsonic incompressible flow

$$\frac{(p_{t_m} - p_m)/p_{t_3}}{(p_{t_3} - p_3)/p_{t_3}} = \frac{q_m}{q_3} = \left(\frac{V_m}{\bar{V}_3}\right)^2$$

and

$$\frac{V_m}{\bar{V}_3} = \left[\frac{(p_{t_m}/p_{t_3}) - (p_m/p_3)(p_3/p_{t_3})}{1 - (p_3/p_{t_3})}\right]^{1/2}$$

where

p_{t_m} maximum value of local total pressure at the survey rake station

p_{t_3} average value of the total pressure at the survey rake station

p_3 average value of the static pressure at the survey rake station

p_m static pressure corresponding to p_{t_m}

$$\frac{p_{t_m}}{p_{t_3}} = \frac{p_{t_m}}{p_{t_\infty}} \frac{p_{t_\infty}}{p_{t_3}}$$

where p_{t_∞} designates the free-stream total pressure.

In ducts where isentropic flow exists somewhere in the streamtube

$$\frac{p_{t_m}}{p_{t_\infty}} = 1.00$$

Also, if the flow is steady and the average Mach number at the rake station is low ($M_3 < 0.30$) $\frac{p_m}{p_3}$ can be assumed equal to 1.00 without appreciable error. Then

$$\frac{V_m}{\bar{V}_3} = \left[\frac{\frac{1}{p_{t_3}/p_{t_\infty}} - \frac{p_3}{p_{t_3}}}{1 - (p_3/p_{t_3})} \right]^{1/2}$$

The ratio of the maximum local velocity to the average velocity is then a function of the average Mach number $\left(\frac{p_3}{p_{t_3}} = f(M_3)\right)$ and the total-pressure ratio p_{t_3}/p_{t_∞}. Since these two variables also determine the duct mass-flow ratio, $m_{2'}/m_{2'}*$, when the duct geometry is known, the velocity ratio $V_m/\bar{V}_3$ can be plotted as a function of mass-flow ratio with the total-pressure ratio as an independent variable (see fig. 7).

REFERENCES

1. Reid, Elliott G.: Performance Characteristics of Plane-Wall Two-Dimensional Diffusers. NACA TN 2888, 1953.

2. Little, B. H., Jr., and Wilbur, Stafford W.: High-Subsonic Performance Characteristics and Boundary Layer Investigation of a 12° 10-Inch-Inlet Diameter Conical Diffuser. NACA RM L50C02a, 1950.

3. Copp, Martin R.: Effects of Inlet Wall Contour on the Pressure Recovery of a 10° 10-Inch-Inlet Diameter Conical Diffuser. NACA RM L51E11a, 1951.

4. Copp, Martin R., and Klevatt, Paul L.: Investigation of High-Subsonic Performance Characteristics of a 12° 21-Inch Conical Diffuser, Including the Effects of Change in Inlet-Boundary-Layer Thickness. NACA RM L9H10, 1950.

5. Fage, A., and Raymer, W. G.: Note on Empirical Relations for a Turbulent Boundary Layer. R and M 2255, British A.R.C., Mar. 6, 1946.

6. von Doenhoff, Albert E., and Tetervin, Neal: Determination of General Relations for the Behavior of Turbulent Boundary Layers. NACA Rep. 772, 1943.

7. Stanitz, John D.: Design of Two-Dimensional Channels with Prescribed Velocity Distributions Along the Channel Walls. I - Relaxation Solutions. NACA TN 2593, 1952.

8. Kantrowitz, Arthur: The Formation and Stability of Normal Shock Waves in Channel Flow. NACA TN 1225, 1947.

9. Ferri, Antonio, and Nucci, Louis M.: The Origin of Aerodynamic Instability in Supersonic Inlets at Subcritical Conditions. NACA RM L50K30, 1951.

10. Lukasiewicz, J.: Diffusers for Small Supersonic Mach Numbers; Design Data. British R.A.E. TN No. Aero. 1973, SD 84, Sept. 1948.

11. Naumann: Diffuser Efficiencies at High Subsonic Velocities. Rep. No. FB 1705, Technical Institute for Aerodynamics, Aachen, Mar. 30, 1943.

12. Seddon, J.: Air Intakes for Aircraft Gas Turbines. Jour. Roy. Aero. Soc., Oct. 1952, pp. 749-787.

13. Garner, H. C.: The Development of Turbulent Boundary Layers. R and M 2133, British A.R.C., June 1944.

14. Wyatt, DeMarquis D.: Analysis of Errors Introduced by Several Methods of Weighting Nonuniform Duct Flows. NACA TN 3400, 1955.

15. Nussdorfer, T. J.: Some Observations of Shock-Induced Turbulent Separation on Supersonic Diffusers. NACA RM E51L26, 1954.

16. Persh, Jerome, and Bailey, Bruce M.: Effects of Surface Roughness Over the Downstream Region of a 23° Conical Diffuser. NACA TN 3066, 1954.

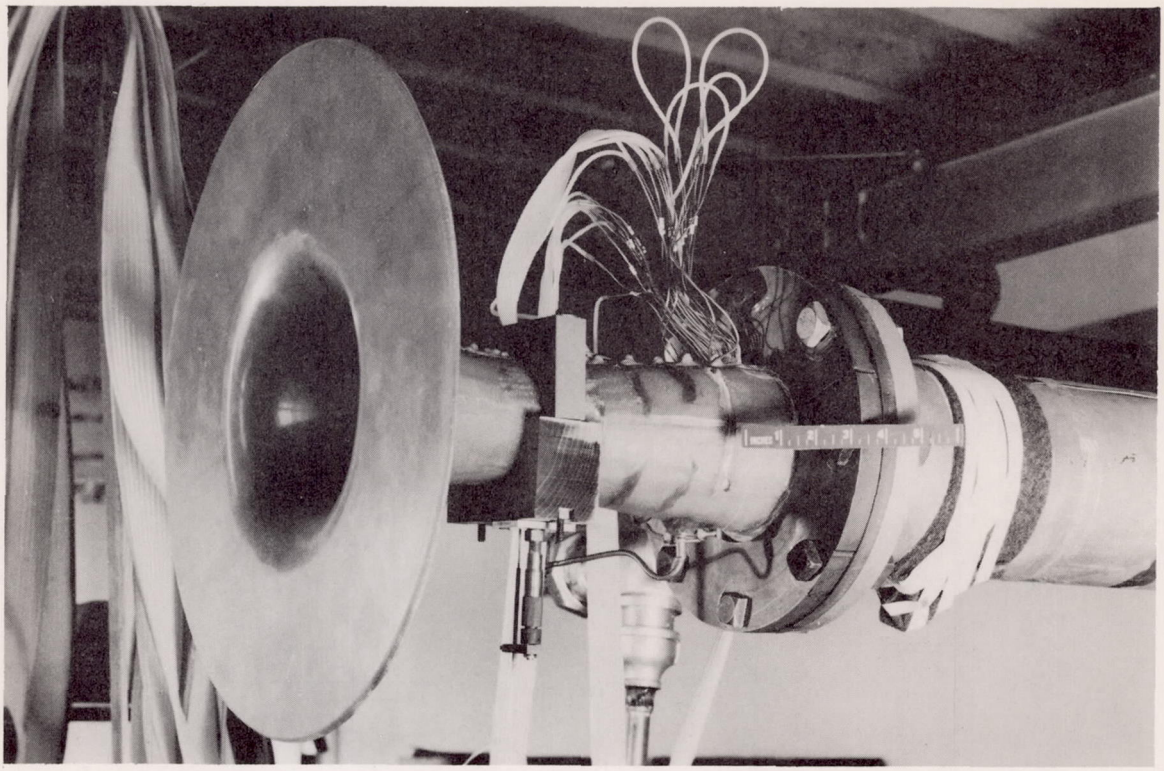

A-20326

Figure 1.- Photograph of test installation.

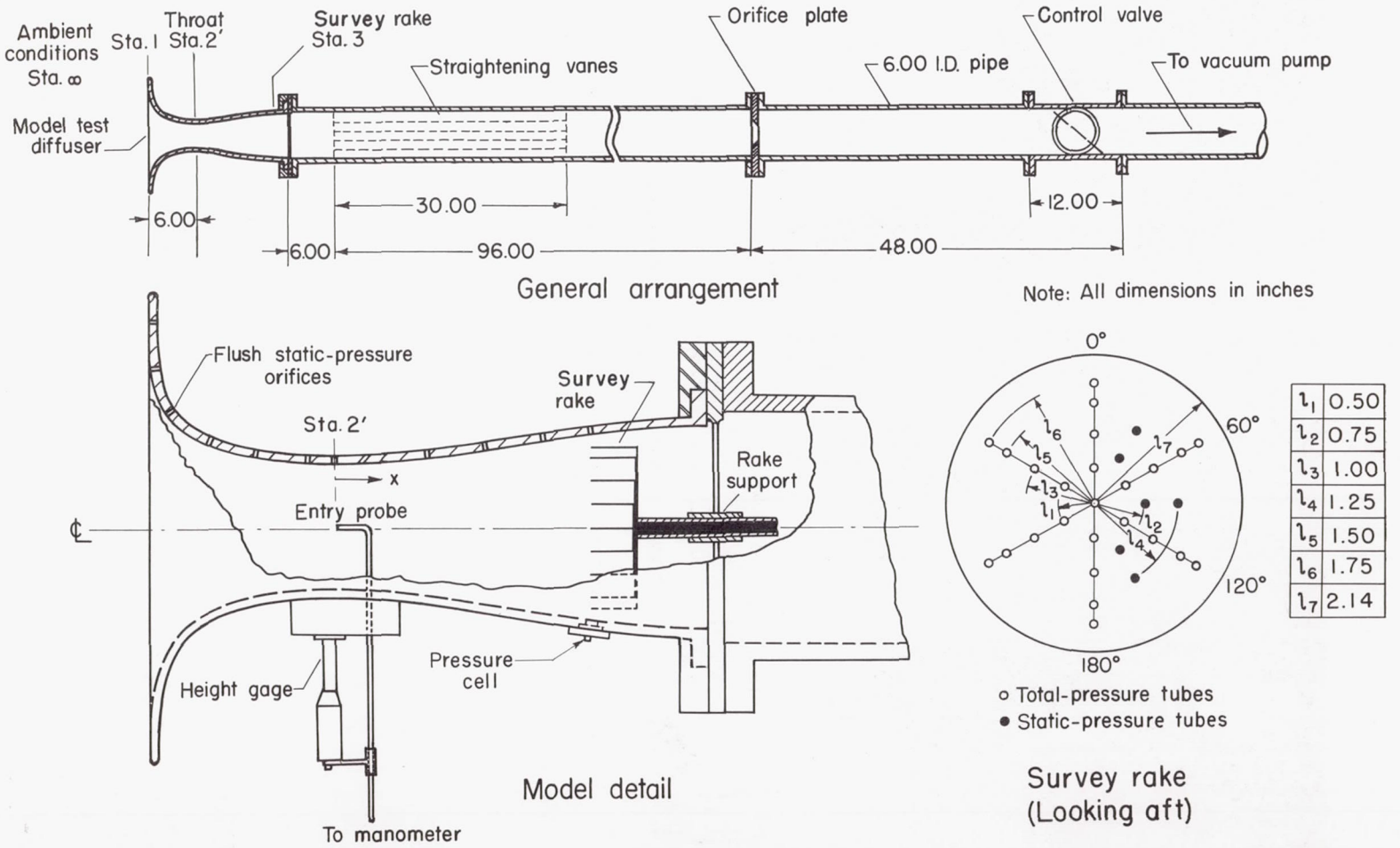

Figure 2.- Sketch showing general test arrangement, and model and instrumentation details.

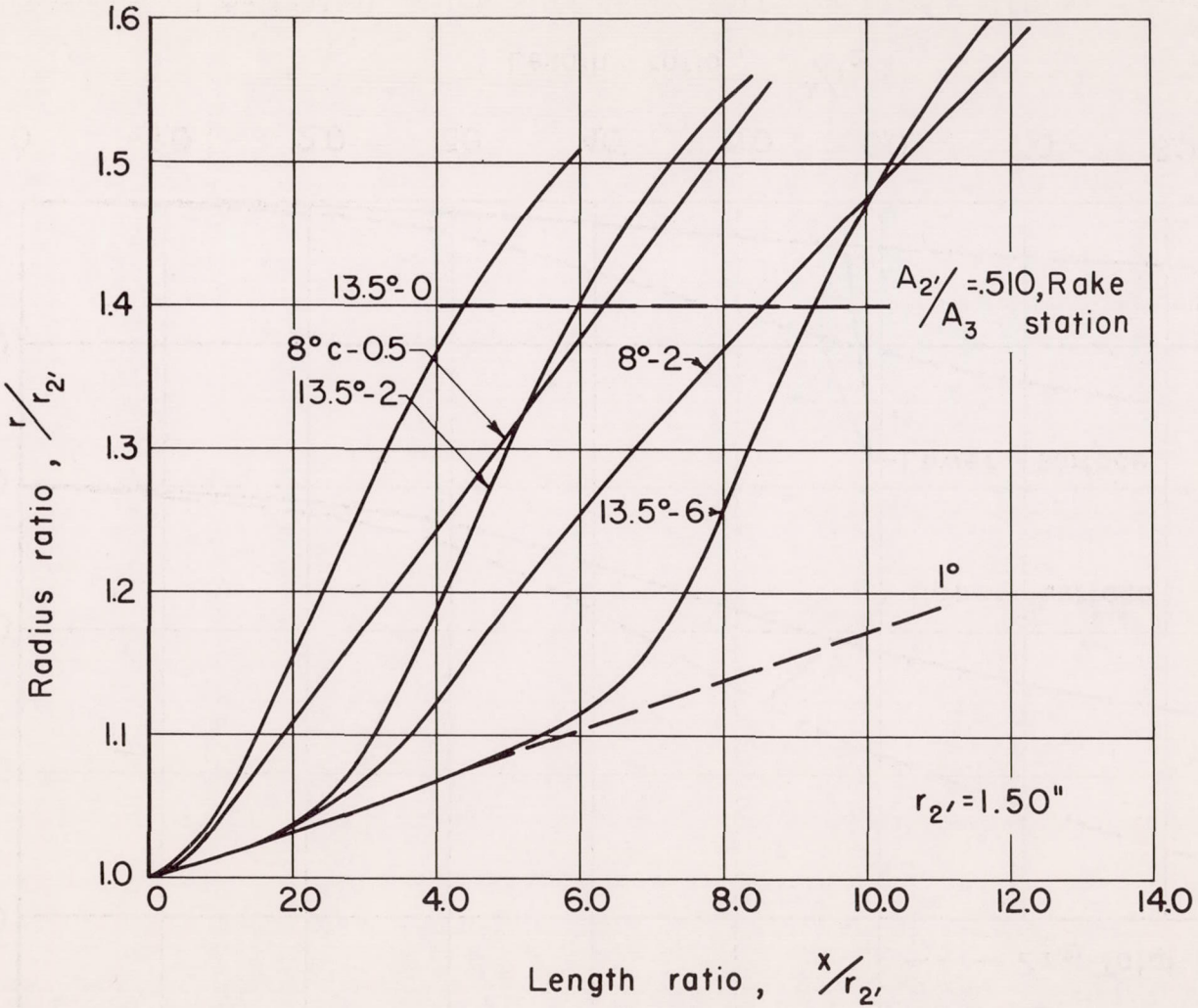

Figure 3.- Longitudinal variation of radius ratio for straight diffuser models.

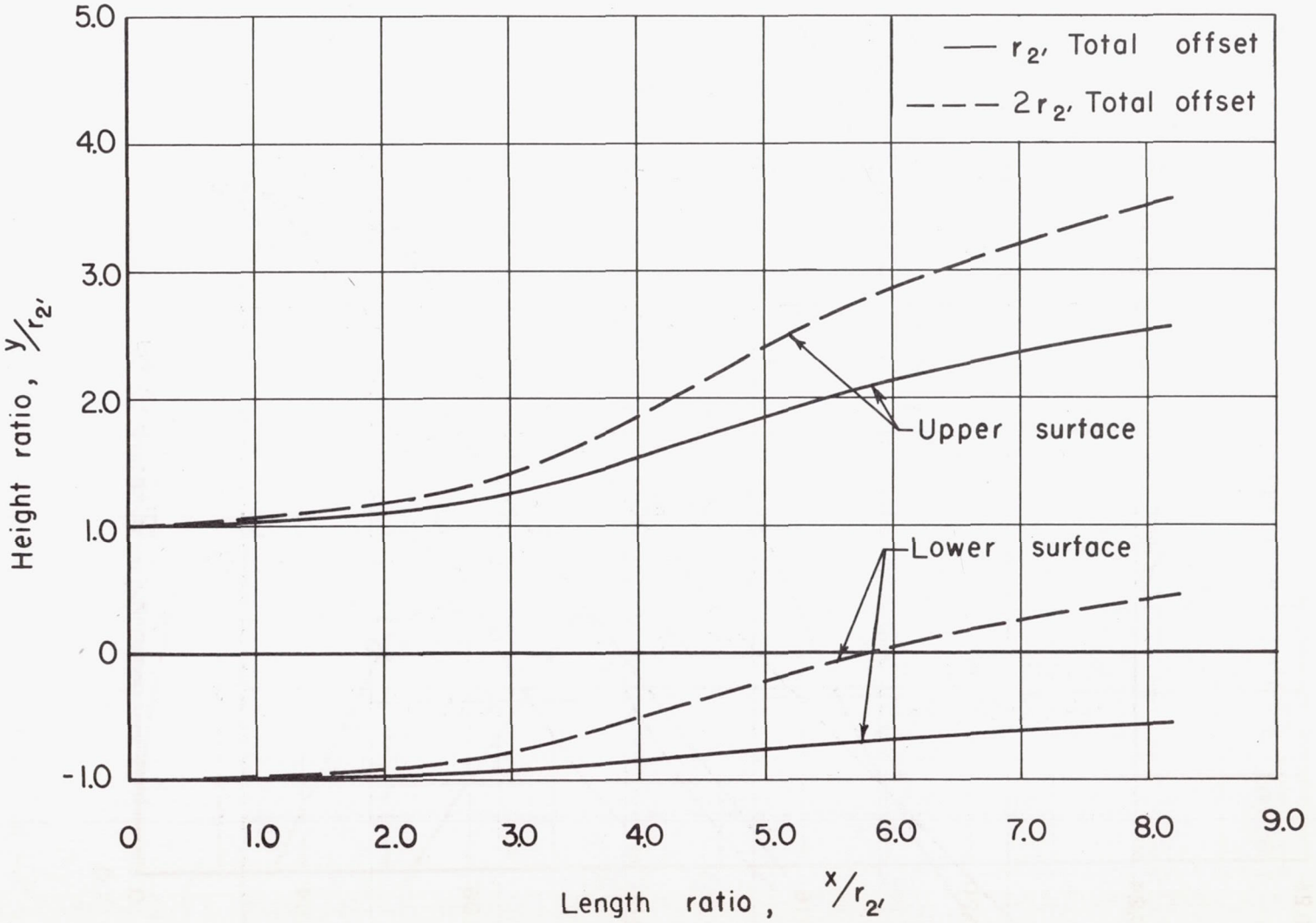

Figure 4.- Longitudinal variation of height ratio for offset diffuser models.

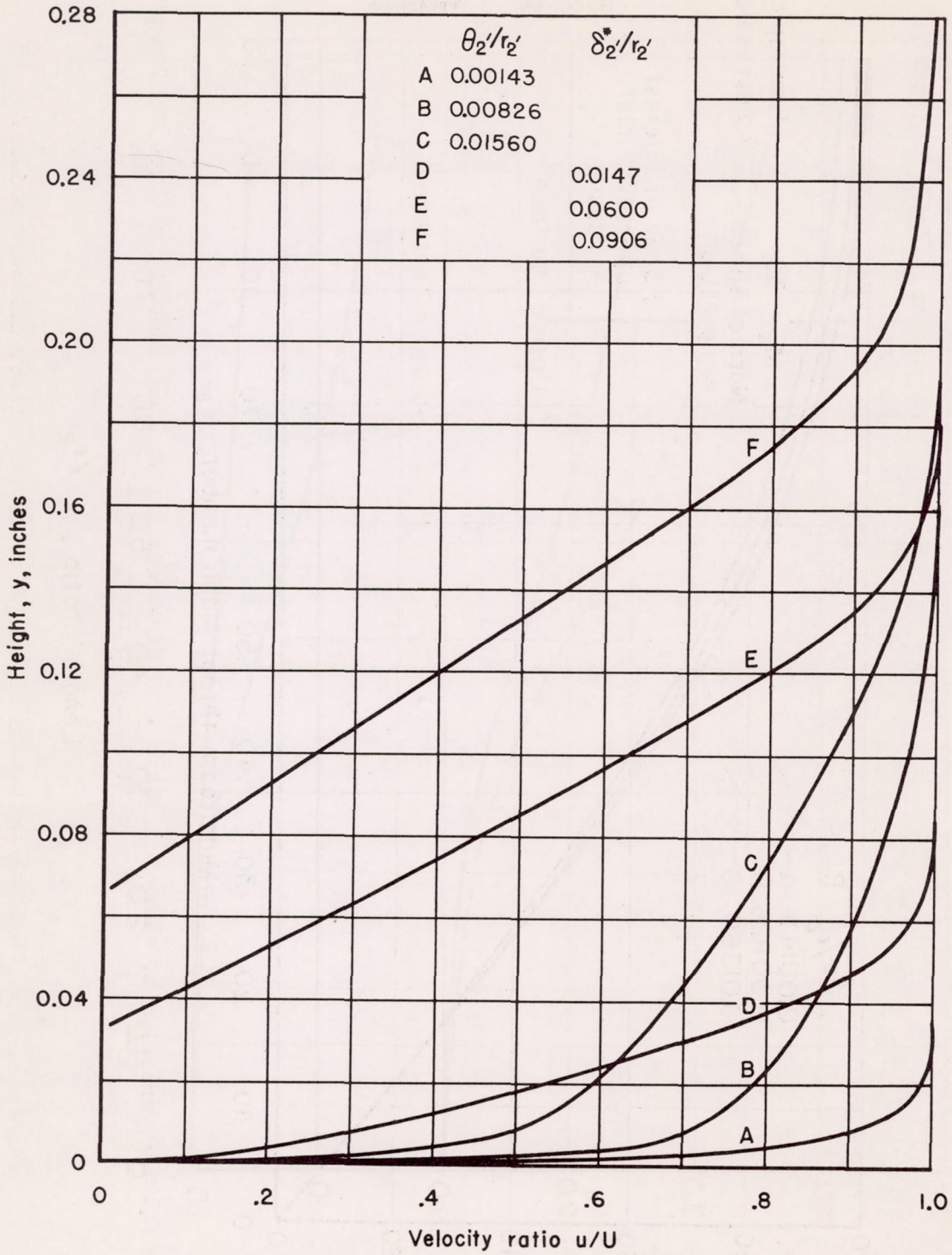

Figure 5.- Boundary-layer velocity profiles representing test conditions at the entrance of the diffuser models.

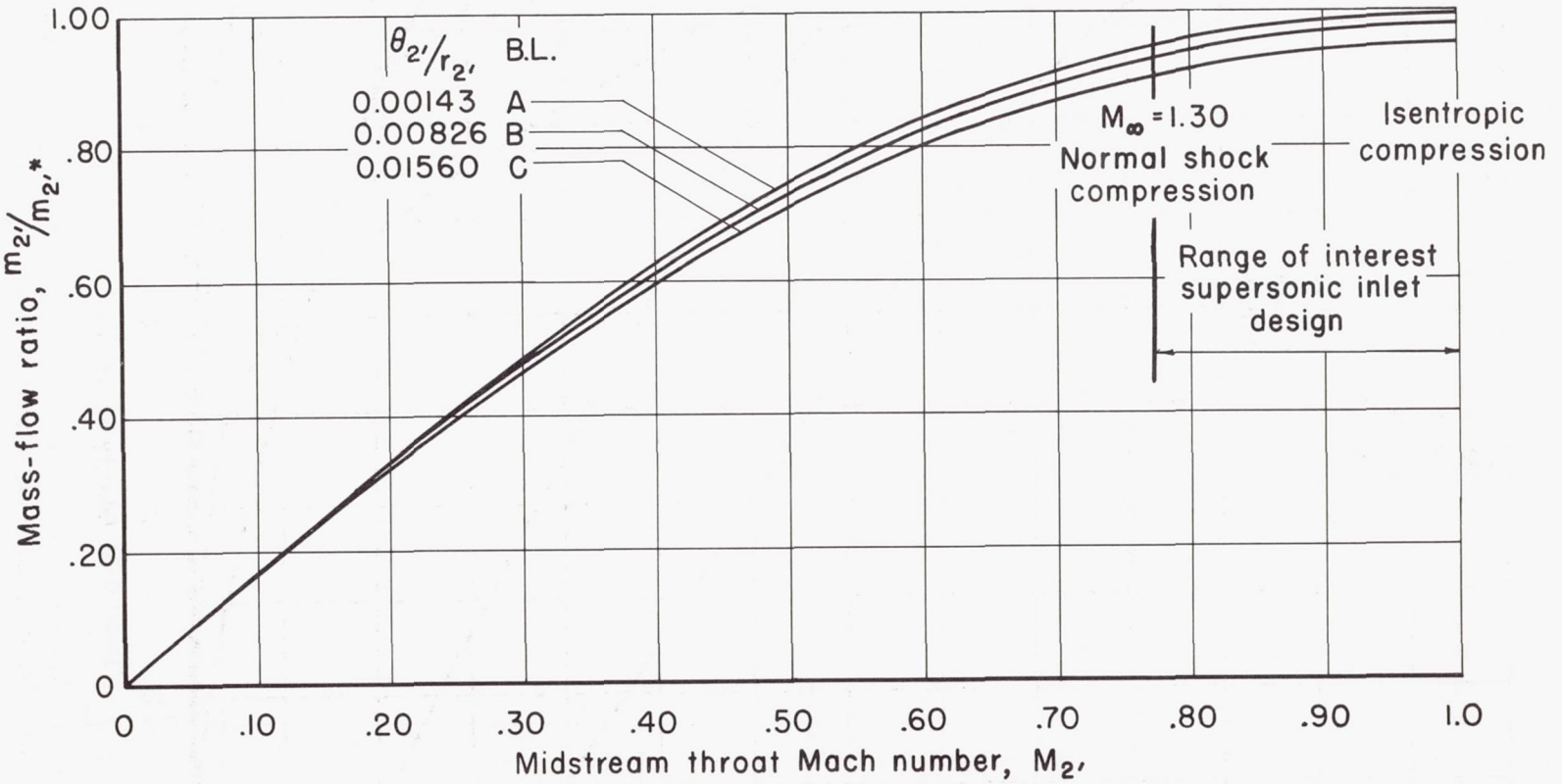

Figure 6.- The variation of mass-flow ratio with midstream throat Mach number for three thicknesses of attached boundary layer.

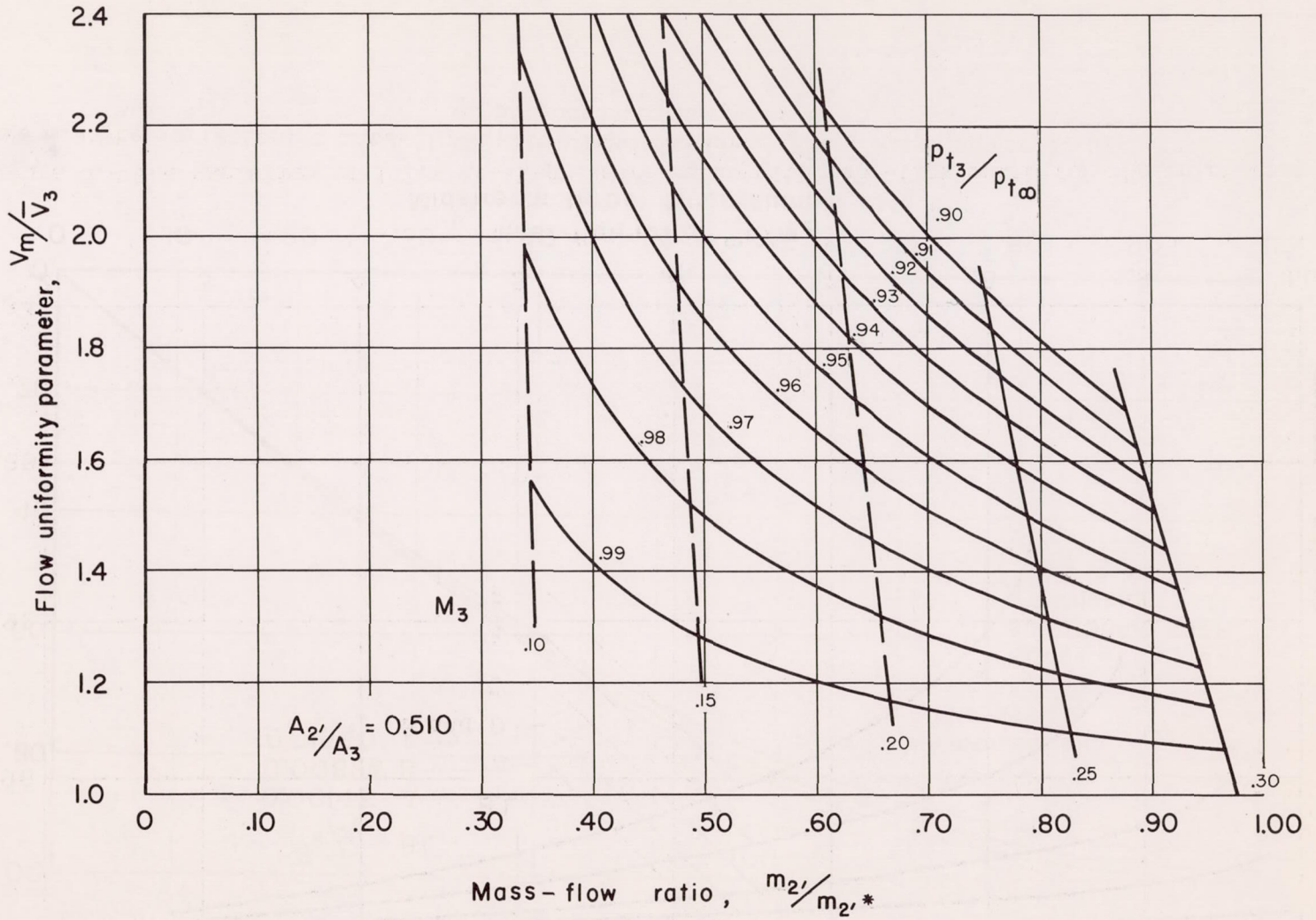

Figure 7.- Flow uniformity parameter as a function of mass-flow ratio and total-pressure ratio.

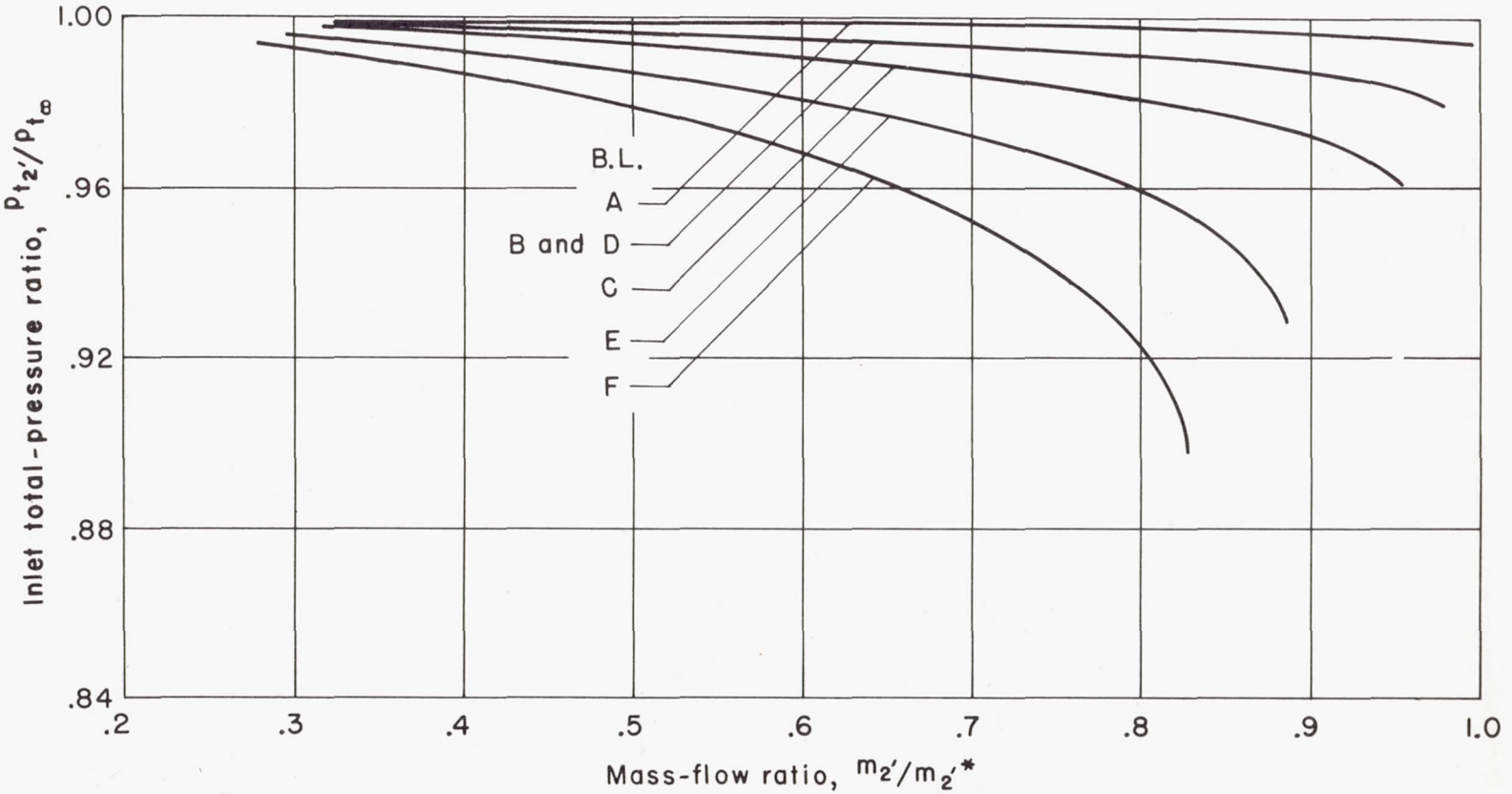

Figure 8.- The variation of inlet total-pressure ratio with mass-flow ratio for the inlet test conditions.

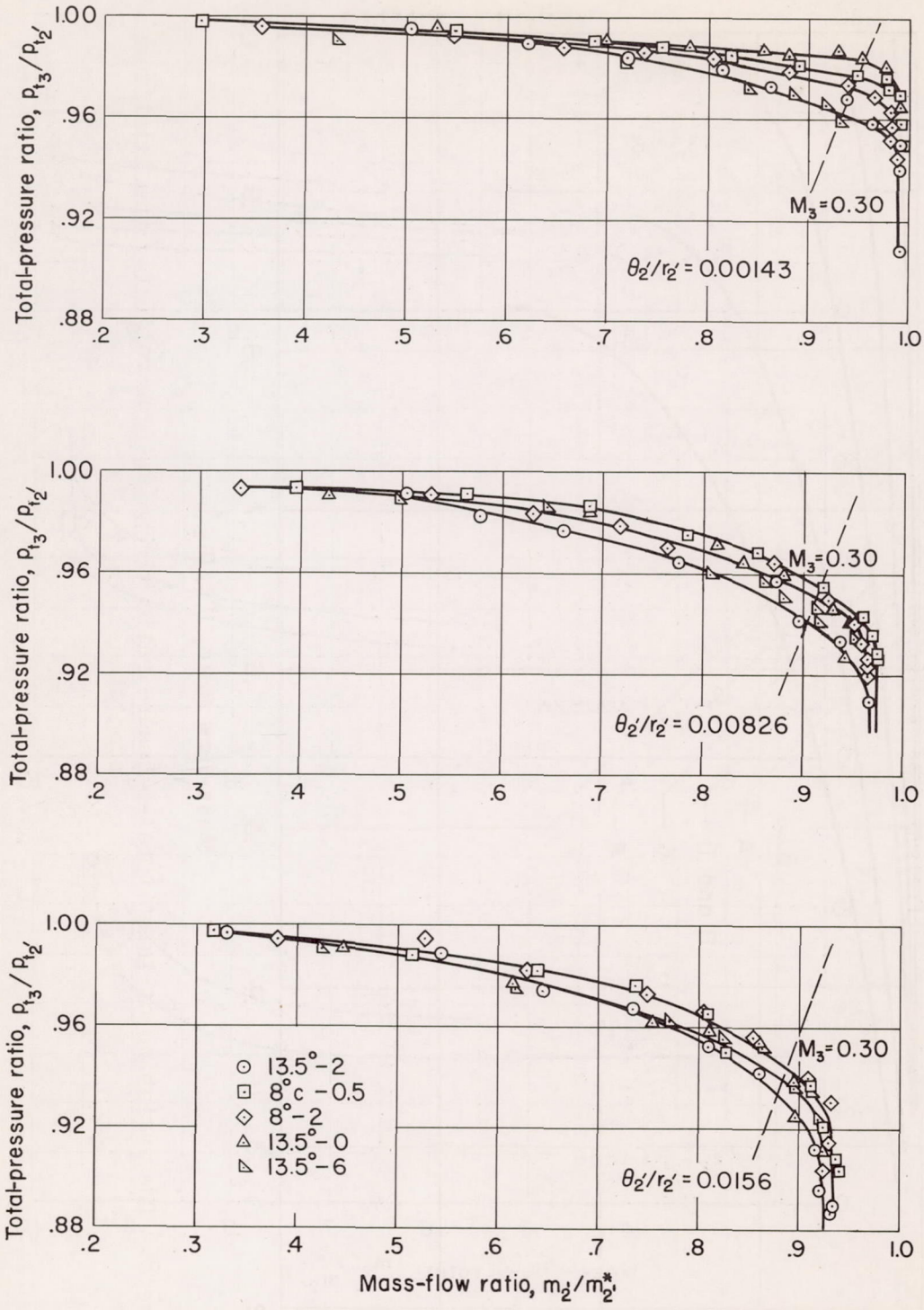

Figure 9.- Total-pressure-ratio characteristics of straight diffuser models for three thicknesses of attached boundary layer.

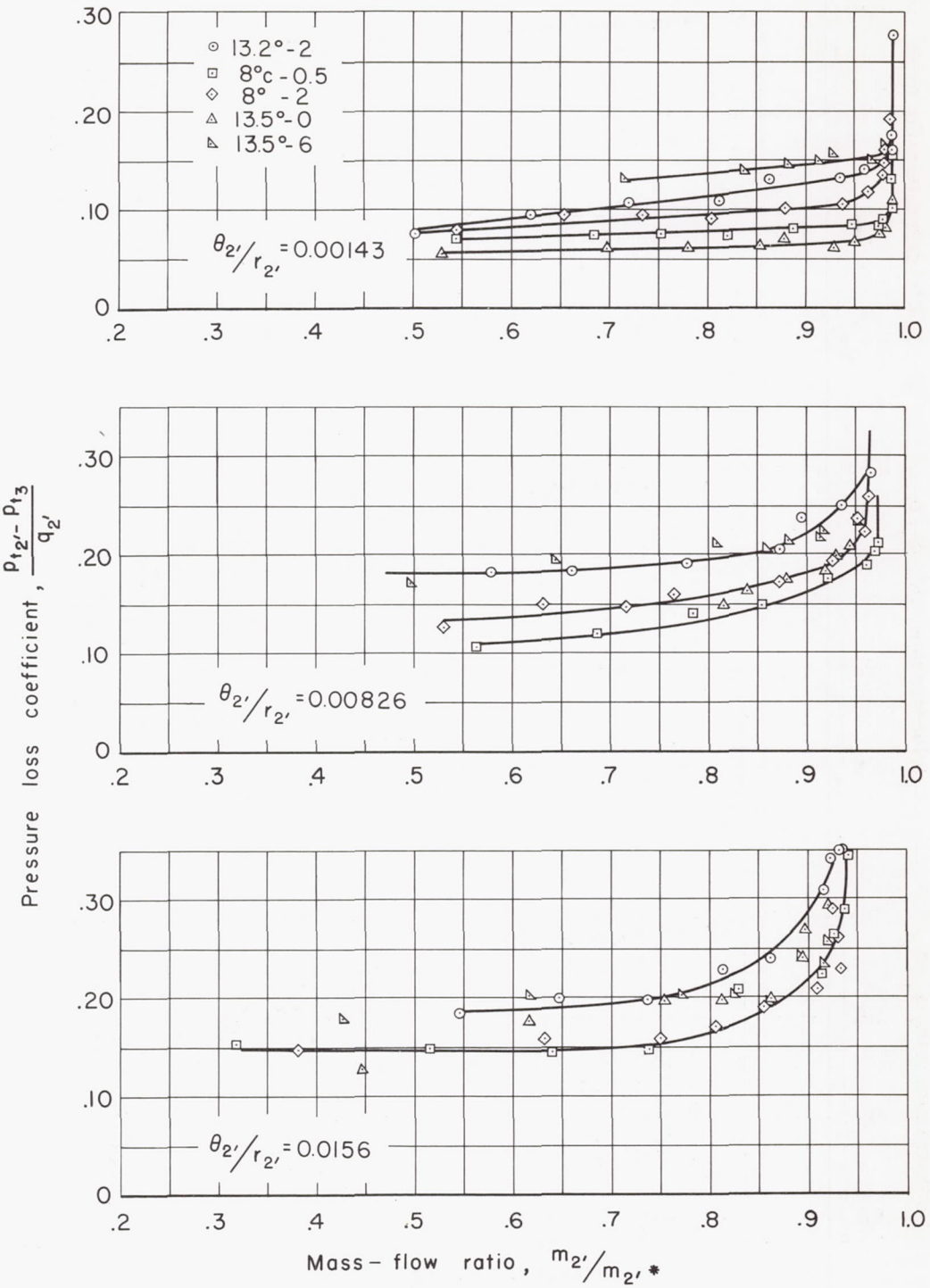

Figure 10.- The variation of pressure loss coefficient with mass-flow ratio for straight diffuser models.

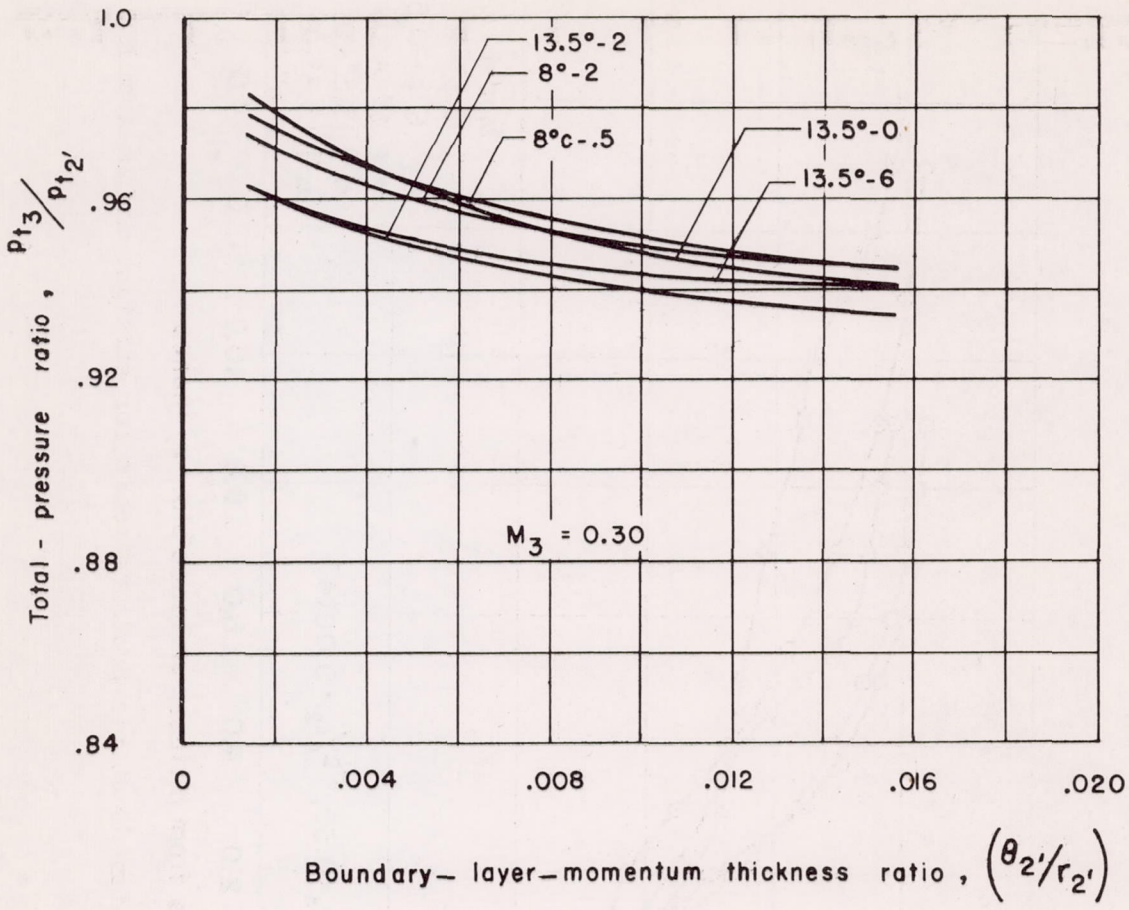

Figure 11.- The variation of total-pressure ratio with momentum thickness ratio for straight diffuser models.

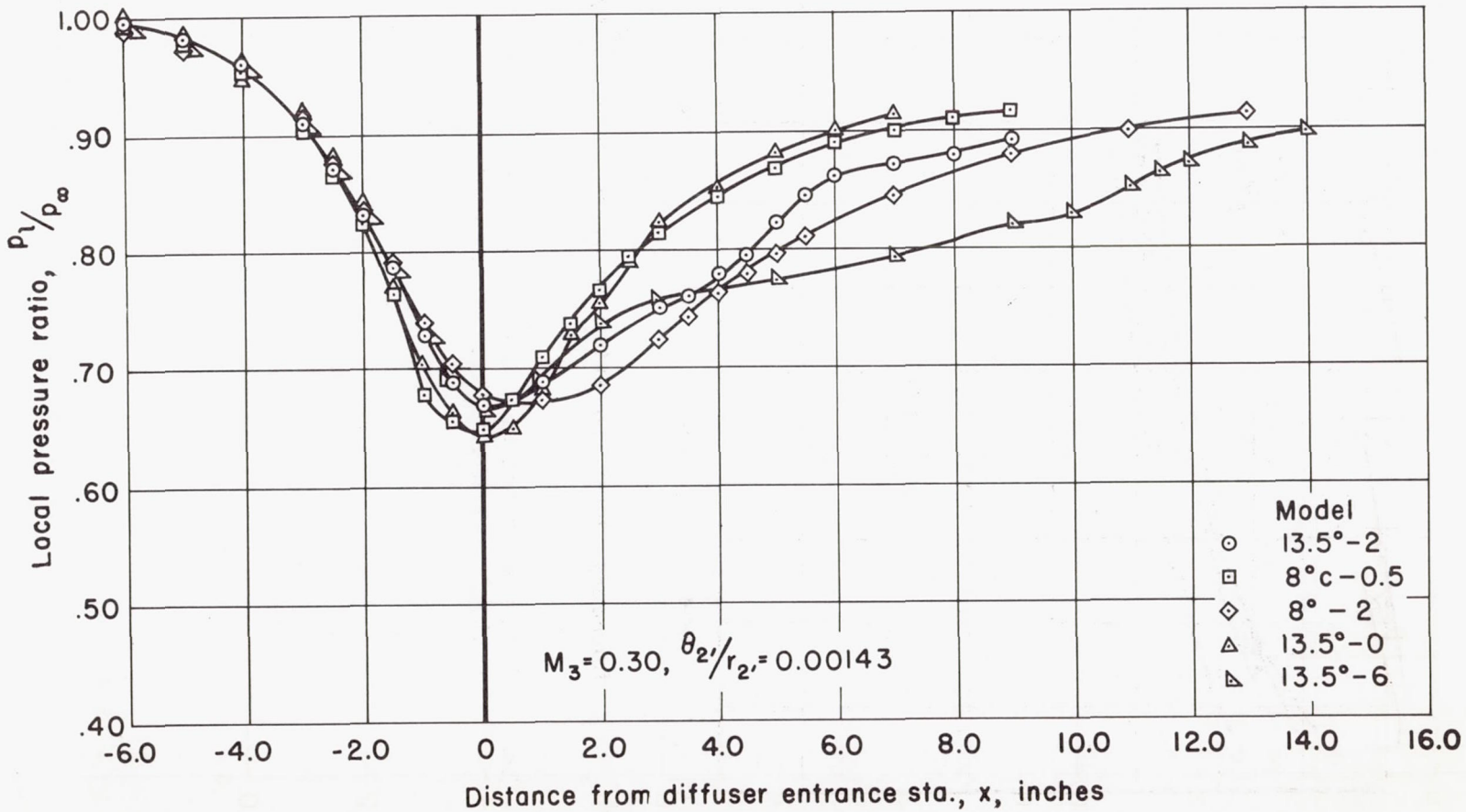

Figure 12.- The longitudinal variation of static-pressure ratio for straight diffuser models.

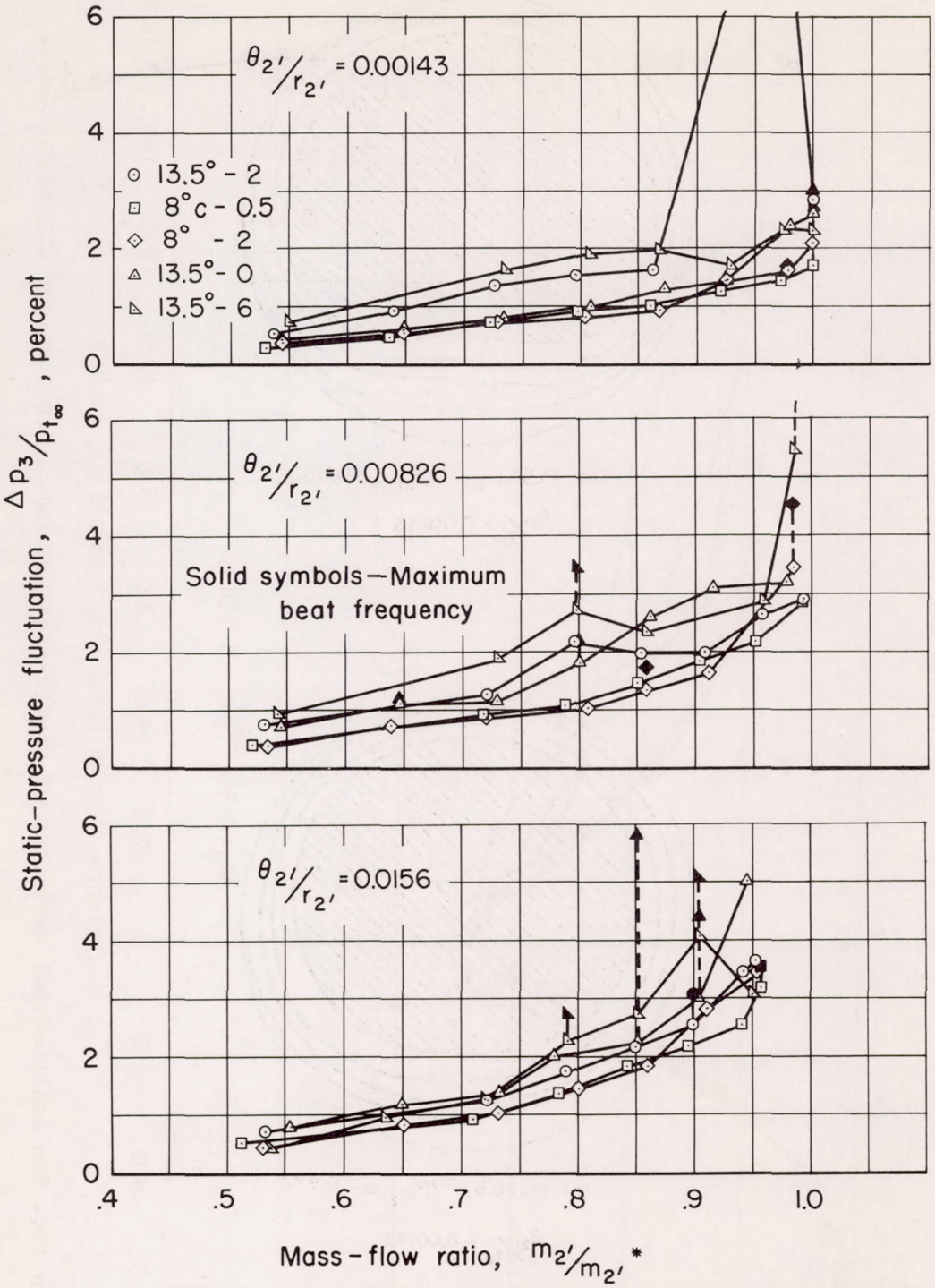

Figure 13.- Static-pressure fluctuation characteristics of straight diffuser models.

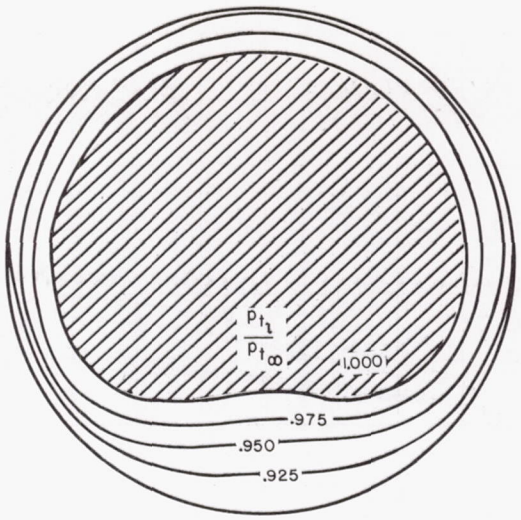

(a) 13.5°-0, $m_{2'}/m_{2',*} = 0.980$

$\theta_{2'}/r_{2'} = 0.00143$

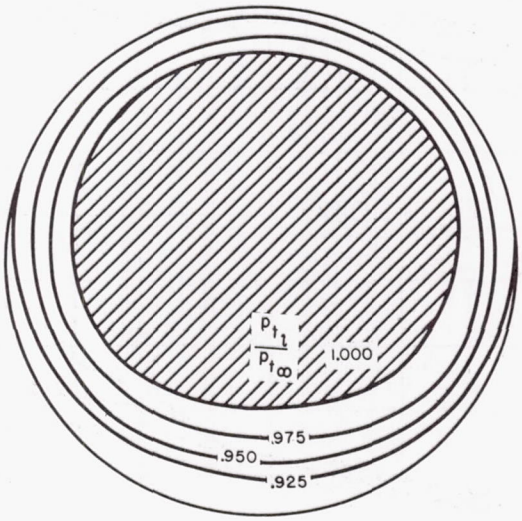

(b) 8°c-0.5, $m_{2'}/m_{2',*} = 0.977$

$\theta_{2'}/r_{2'} = 0.00143$

Figure 14.- Total-pressure-ratio profile characteristics of two straight diffuser models.

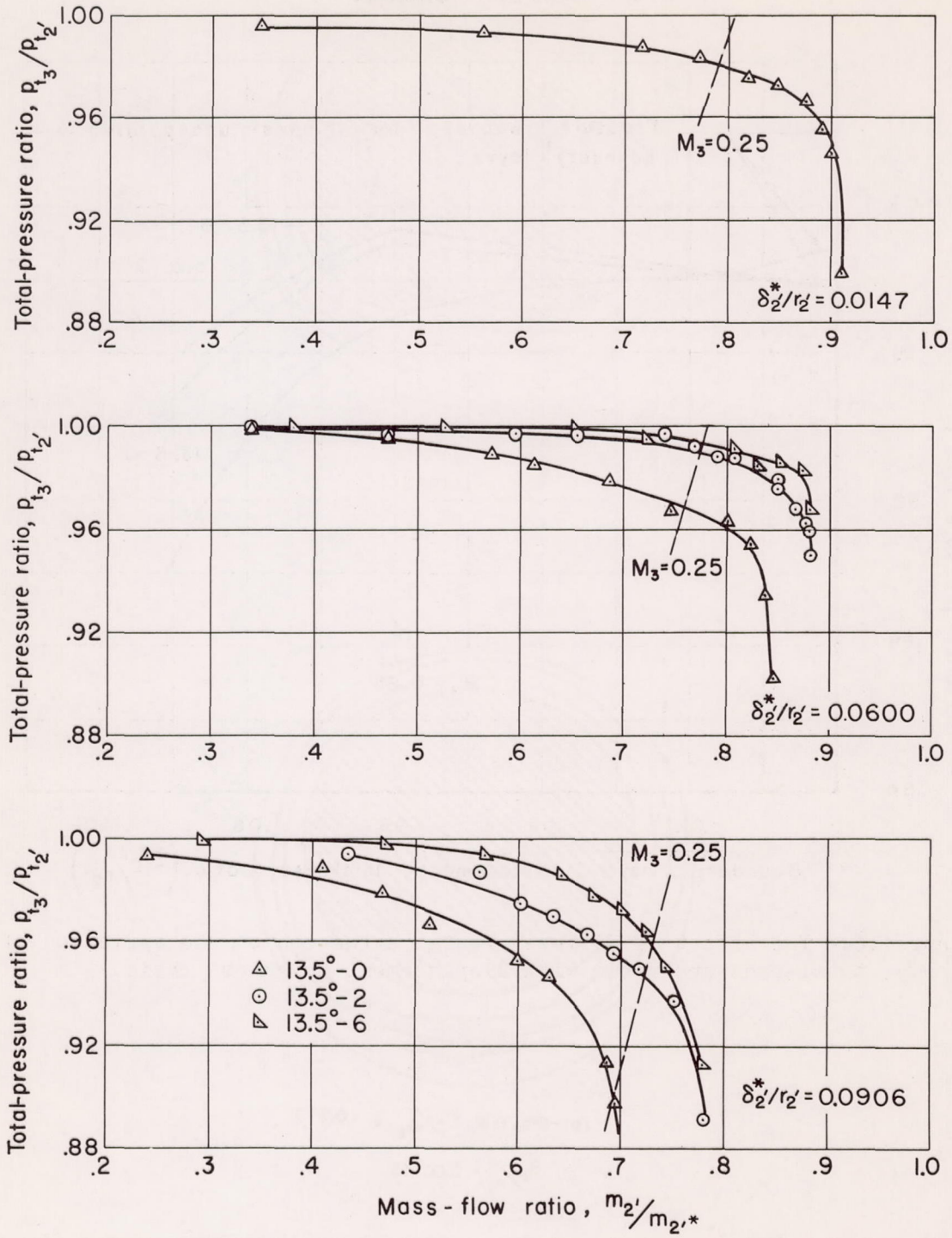

Figure 15. - The effect of diffuser throat extension on total-pressure ratio for three thicknesses of separated boundary layer.

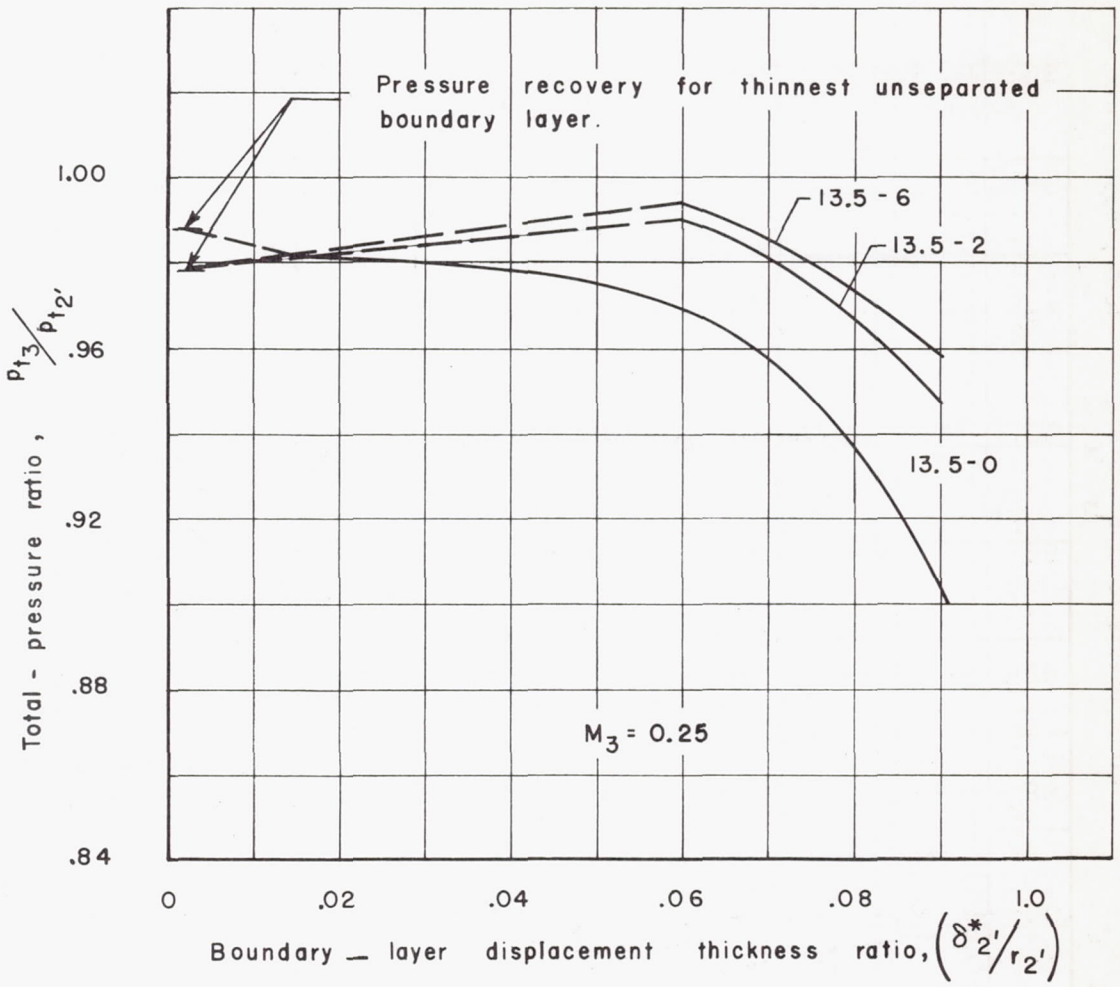

Figure 16.- The effect of diffuser throat extension on the variation of total-pressure ratio with displacement thickness ratio.

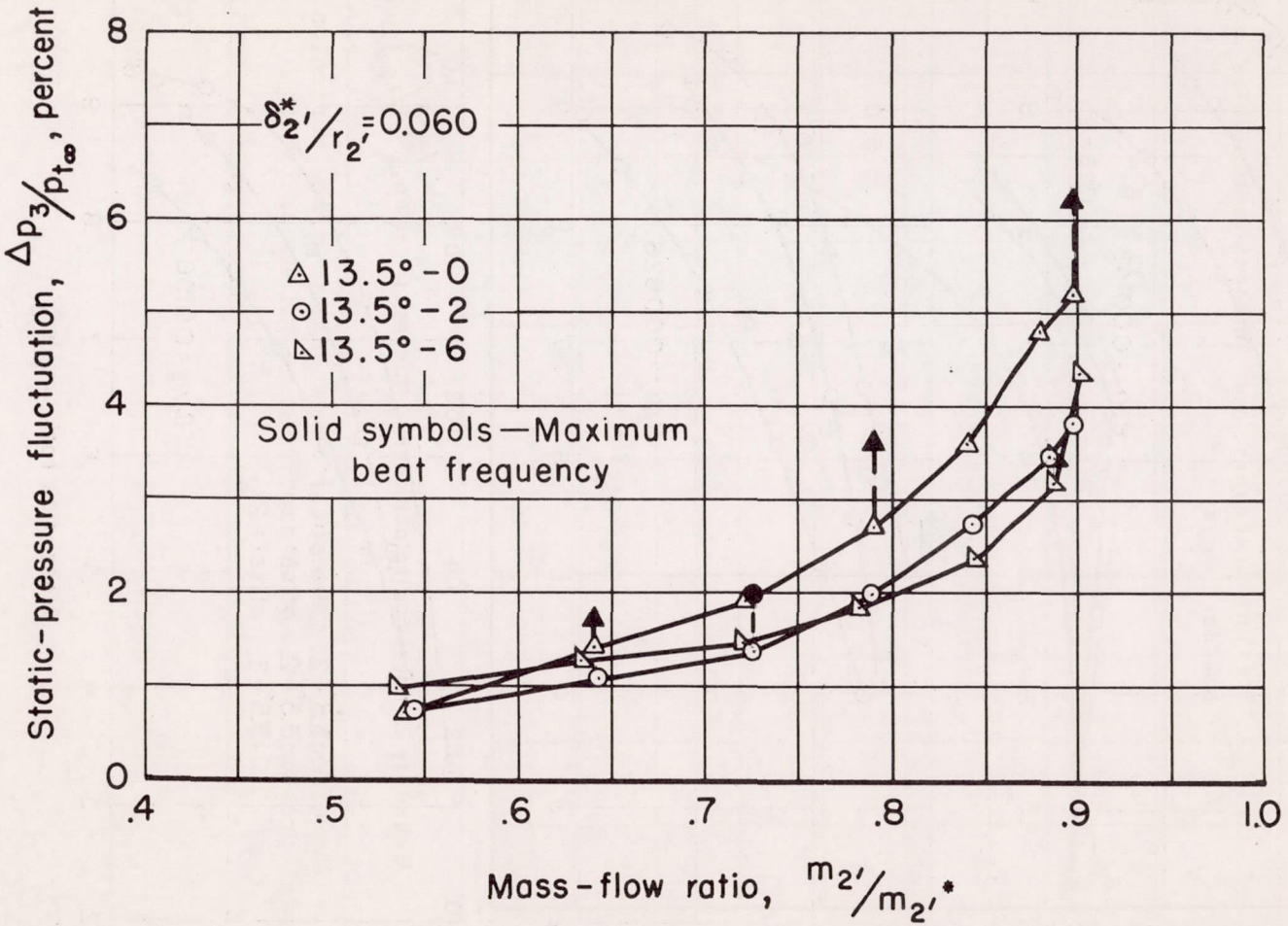

Figure 17.- The effect of diffuser throat extension on static-pressure fluctuation.

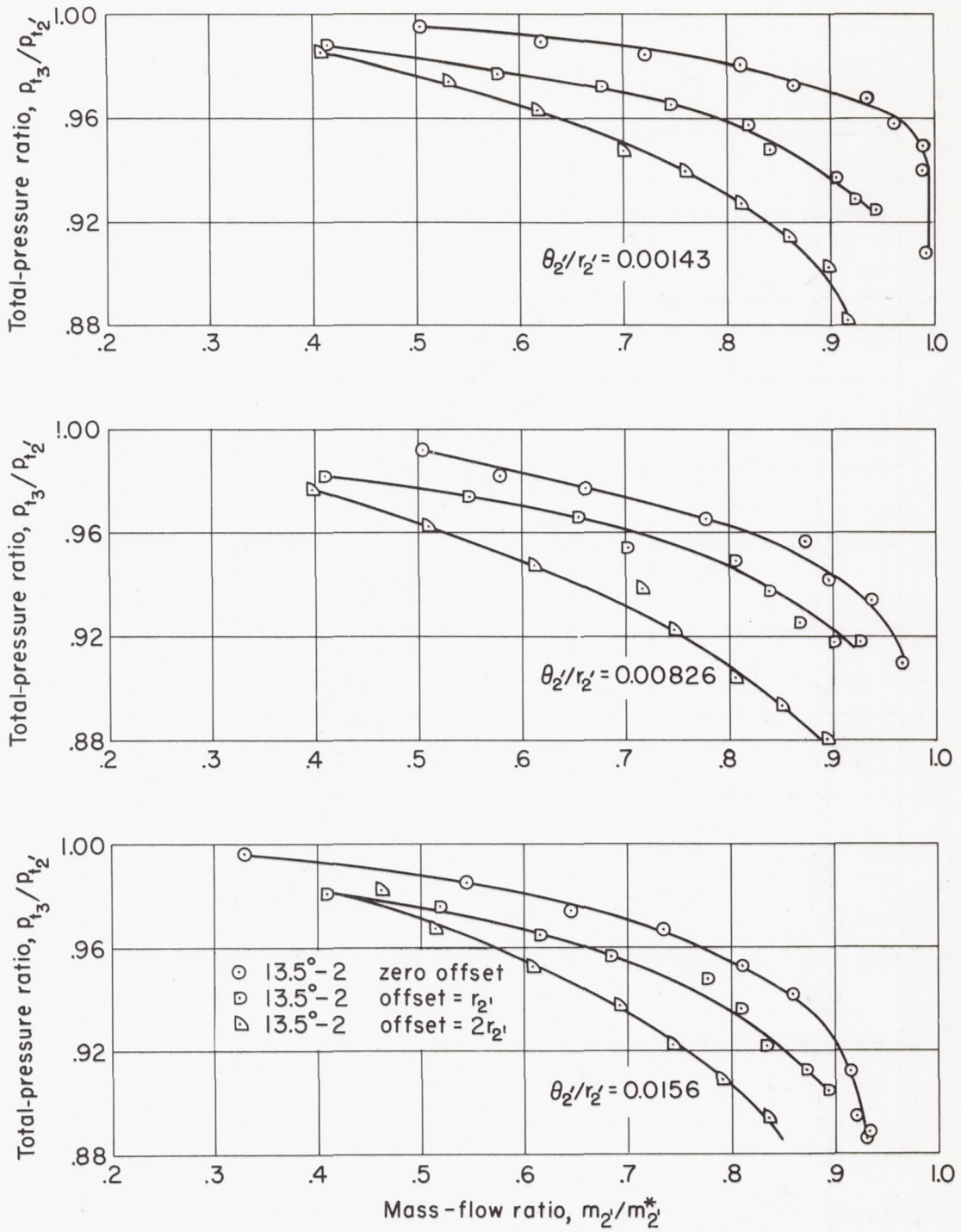

Figure 18.- Total-pressure-ratio characteristics of offset diffuser models for three thicknesses of attached boundary layer.

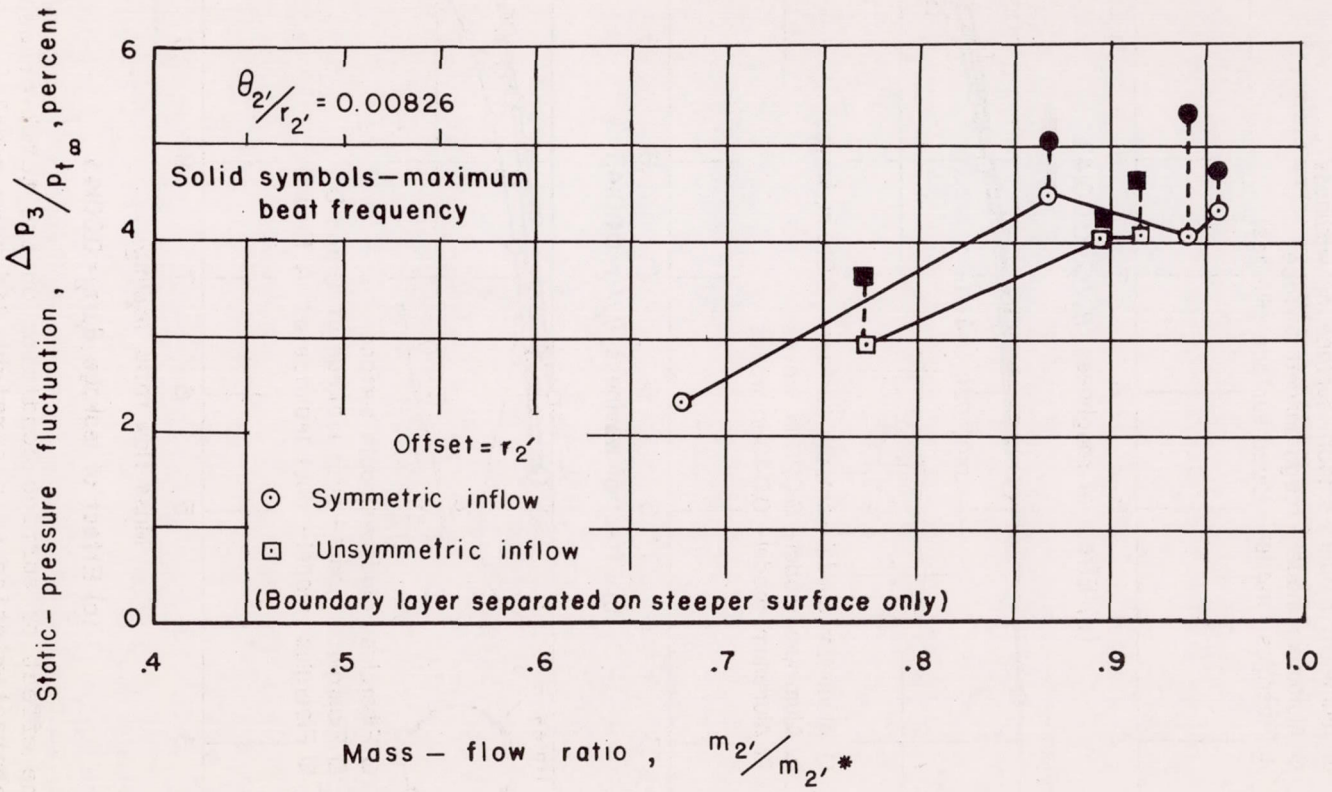

Figure 19.- Static-pressure fluctuation characteristics of offset diffuser models.

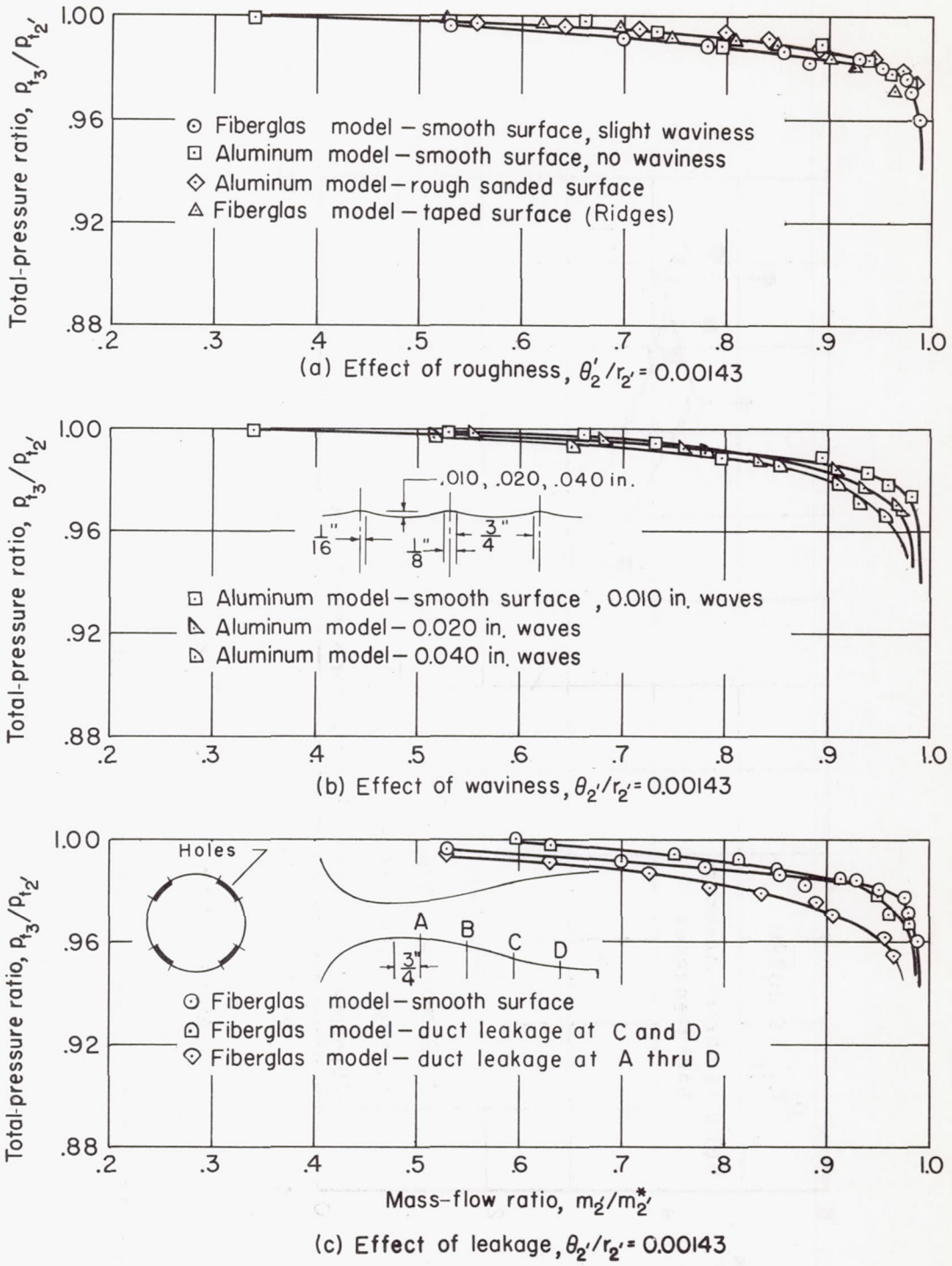

Figure 20.- The effect of surface condition on the total-pressure-ratio characteristics of a straight diffuser model.

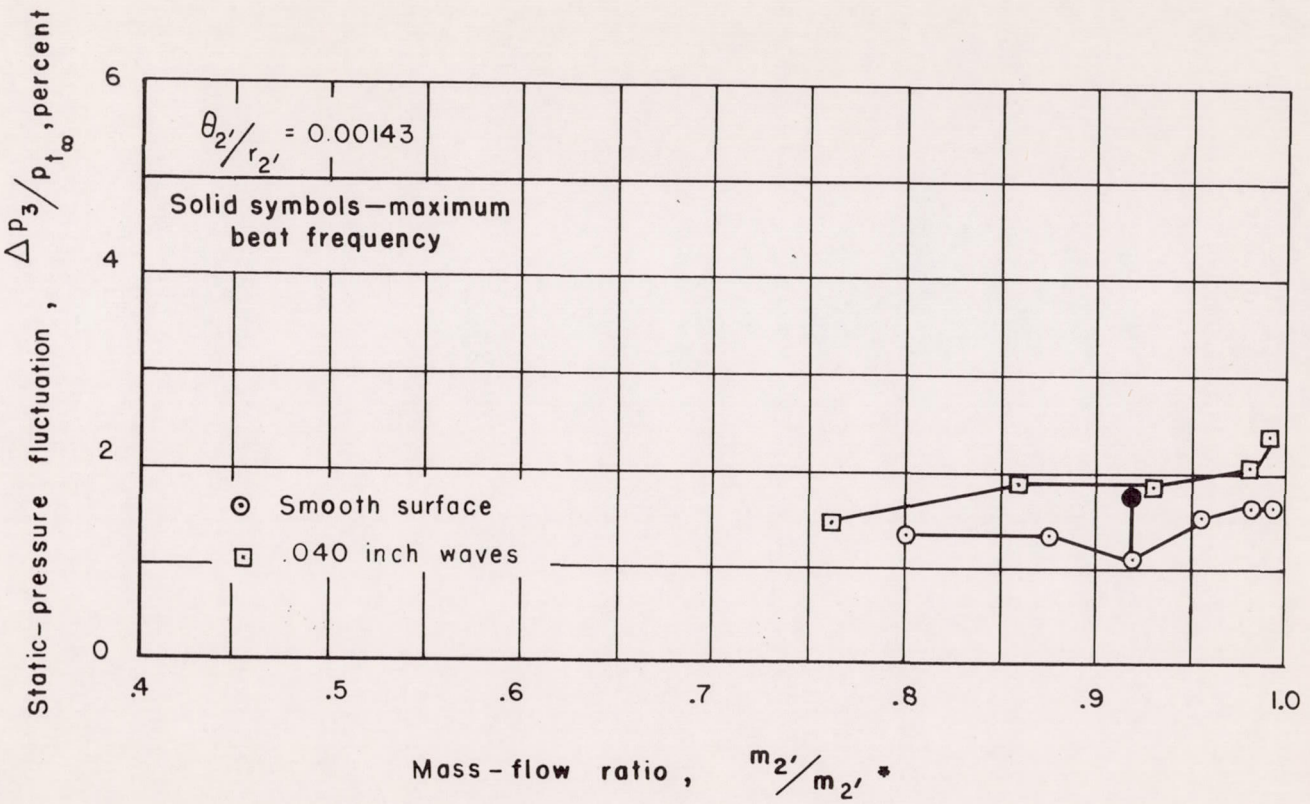

Figure 21.- The effect of surface waviness on the static-pressure fluctuation characteristics of a straight diffuser model.